CURRENT MEASUREMENT IN POWER ELECTRONIC AND MOTOR DRIVE

APPLICATIONS – A COMPREHENSIVE STUDY

by

ASHABEN MEHUL PATEL

A THESIS

Presented to the Faculty of the Graduate School of the

UNIVERSITY OF MISSOURI-ROLLA

In Partial Fulfillment of the Requirements for the Degree

MASTER OF SCIENCE IN ELECTRICAL ENGINEERING

2007

Approved by

_____   _____
Dr. Mehdi Ferdowsi, Advisor   Dr. Keith Corzine

_____
Dr. Badrul Chowdhury

ABSTRACT

Current measurement has many applications in power electronics and motor drives. Current measurement is used for control, protection, monitoring, and power management purposes. Parameters such as low cost, accuracy, high current measurement, isolation needs, broad frequency bandwidth, linearity and stability with temperature variations, high immunity to dv/dt, low realization effort, fast response time, and compatibility with integration process are required to ensure high performance of current sensors. Various current sensing techniques based on different physical effects such as Faraday's induction law, Ohm's law, Lorentz force law, magneto-resistance effect, and magnetic saturation are studied in this thesis. Review and examination of these current measurement methods are presented.

The most common current sensing method is to insert a sensing resistor in the path of an unknown current. This method incurs significant power loss in a sense resistor at high output currents. Alternatives for accurate and lossless current measurement are presented in this thesis. Various current sensing techniques with self-tuning and self-calibration for accurate and continuous current measurement are also discussed. Isolation and large bandwidth from dc to several kilo-hertz or mega-hertz are the most difficult, but also most crucial characteristics of current measurement. Electromagnetic-based current sensing techniques, which are used to achieve these characteristics, are analyzed. Many applications require average current information for control purposes. Different average current sensing methods of measuring average current are also reviewed.

ACKNOWLEDGEMENT

TABLE OF CONTENTS

LIST OF ILLUSTRATIONS

LIST OF TABLES

1. INTRODUCTION

To be able to control, protect, or monitor a system, certain information about the system is required. In electrical systems this information mainly consists of instantaneous, peak, or average values of the voltage and current signals. Hence, accuracy of current measurement plays an important role in the dynamic performance, efficiency, and safety of an electrical system. Knowing the current information about a system is also important for power management purposes. Applications of current sensing in motor control and power conversion are the main focal points of this thesis. Several detailed descriptions of such systems are provided in the following sub-sections.

1.1. MOTOR DRIVES

Motor current is used as a control variable in motor drives. Vector control and direct torque control require current sensing for control purposes [1-8]. Speed sensorless and voltage sensorless control approaches require motor current measurement to provide accurate control with lower cost, noise, and complexity. Motor current measurement is also required to remove torque ripple in order to provide smooth torque [9, 10]. Modern motor drives are beginning to be digitally controlled and the control elements of such drives require accurate motor current feedback. Therefore, current sensing is of great importance to digitally controlled ac motor drives [11]. Current controlled pulse width modulation (PWM) inverters are used to serve as ac drives. These controllers are classified as hysteresis, ramp comparison, and predictive controllers, all of which require motor current information to determine inverter switching states [12]. Furthermore, information of stator parameters is important for several control schemes. Stator current

measurement is used for the estimation of these parameters [13]. Stator current information is also used for rotor velocity tracking control instead of measuring both rotor flux and velocity [14].

Motor current information is also required to detect rotor position and to check the motor's insulation condition in several applications. Starting from an unknown rotor position may create temporary reverse rotation or starting failure in permanent magnet motors, which is not acceptable in many applications. Rotor position can be detected by using phase current information [15]. Electrical insulation is the most critical component for operation of electrical motors. Stator insulation failure during motor operation can lead to motor failure, resulting in a costly outage. Insulation condition indicators such as capacitance and dissipation factor are calculated based on the measurement of the differential leakage currents of each phase winding [16].

Current sensing is also important for safety and efficient regulation of all the equipment using industrial motor drives, for example, a motor which is used to open and close elevator doors. An elevator door must react to an object or a person hindering closure. The obstacle detection in the elevator is performed by sensing motor currents. The obstacle creates higher torque, which causes higher currents in the motor. This current information is used to trigger the signal to open the door. Motor current measurement is also important for the elevator's smooth acceleration and stopping and for placing the cabin exactly level to its destination [17]. Another example is speed control in a forklift. The motor in the forklift is required to adjust the speed and the ascending and descending of the fork. For smooth and steady forklift operation, motor current information in the forklift is required to lift the fork with the same precision and

speed regardless of the amount of load it needs to transport. By measuring the motor current, the forklift adjusts the power required to perform the task.

1.2. POWER ELECTRONIC CONVERTERS

A current sensor in a power electronic converter is used to measure the constantly varying current in order to provide feedback for control purposes. This leads to the accurate and smooth adjustment of converter operation. Current-mode control is implemented in converters to regulate the output voltage. Current-mode control approaches for converters are classified as peak, average, valley, hysteretic, PWM conductance, and output current feed-forward control. All current-mode control types require inductor waveform information to provide appropriate transient response [18-23].

Current sensing in converters is also required for mode hoping, current sharing, ripple cancellation, and integrated power electronic modules (IPEMs). In mode hoping, the sensed converter current is used to determine when to switch between continuous conduction mode and discontinuous conduction mode [24]. Current information is required for current sharing in parallel or multi-phase converters so that the stress among the paralleled dc–dc converters is balanced [25]. In some applications, an active ripple filter is required in power electronic converters to cancel the current ripple [26]. This active ripple filter requires information about converter current. IPEMs are used in vehicles to reduce cost, package size, and interconnect. Current sensing is the most important requirement for an IPEM [27, 28].

Converter current information is also important for power generation applications, for example, inverters used in gas co-generators. In gas co-generators, gas is used to produce steam to drive the turbine to produce electricity through an inverter. This inverter

is directly connected to the household electrical network. To ensure that the output of the inverter is perfectly matched with the electrical network, the output current of the inverter must be known. The grid needs to be supplied with continuous power at a controlled frequency and voltage [29]. Another example is wind generation. The electricity produced by on-shore or off-shore wind turbine generators needs to be safely fed into the grid. To do so, it is required to transform and optimize the generation of electricity from the wind turbine. Current measurement is required for every converter in wind energy turbines to enable optimal control and protection. Current sensors also continuously measure the current in the converters to position the turbine in relation to the wind [30].

1.3. PROTECTION AND MONITORING

Protecting supply circuits against overloading conditions requires the system to sense its current delivery. The over current is a severe fault situation that can result in the failure of the device if appropriate action is not taken in time. The over current is caused by a short circuit, malfunction, or component failure. Current sensing is required for fault detection and its minimization [31, 32]. It enables emerging state-of-art switching supplies to improve transient response, efficiency, and compensation performance [33]. Current measurement is also required for ground fault detection on power lead for personnel protection. The safety lights on airport runways, towers, and chimneys require continuous current sensing.

Furthermore, current monitoring is required for process control, maintenance, and infrastructure management. Current consumption by industrial heaters, electroplating processes, smelting furnaces, electrolysis processes, electric dip coatings, etc, needs to be monitored for process control. A motor supplying a cutting tool drawing too much

current indicates that the cutting tool is blunt and needs to be sharpened or replaced. In air conditioning, ventilation, and heating applications, the contamination amount on an air filter is determined from the amount of current consumed by the fan's electric drive.

1.4. BATTERY APPLICATIONS

Power management in vehicles includes battery management, battery's state of heath, and auto-disconnection of a battery; all of which require battery current information.

Battery current information is important in finding battery's state of charge (SoC) [34-36]. A battery's SoC is defined as its available capacity as a percentage of its rated capacity. Finding the SoC during fast charging in Ni-MH (nickel-metal hydride) battery prevents oxygen production under high charging currents. Only 10% oxygen generation will create 5-6 times more heat than normal operation. SoC information is also required to avoid the extreme operating conditions such as fully charged and fully discharged conditions.

1.5. SELECTION CRITERIA

There are many issues that need to be considered when choosing a current sensor for a particular application. The designer needs to think about all aspects of an application. Table 1.1 lists all the criteria which require special consideration while selecting a current sensor [37].

Table 1.1. Selection criteria for a current sensor

Parameters	Types	Criteria
Electrical	Current types	dc, ac, and complex
	Voltage	Primary working voltage, dielectric withstand voltage, compliance to the relevant standards, applicable standard for isolation, over voltage category, impulse withstand voltage, single or reinforced insulation
	Ranges	Nominal current, peak current, transient current, maximum peak value
	Required output signal	Output value at nominal or peak current, selection of desired or necessary output load impedance
	Measurement accuracy	Required accuracy at 25°C (ambient temperature), dc offset and non linearity of the output signal, global accuracy within the operating temperature range, the offset drift, and the gain drift
	Available power supply	Power supply voltage, maximum allowable current consumption
Environmental	Temperature	Extreme storage temperature, minimum and maximum working temperatures
	Presence of external field	Fields from transformers or inductors, magnetized materials in the area, other currents similar or greater amplitude, external current identical to the measured one
	Vibration and shock	Standards and levels to be considered
Dynamic	di/dt	Match between di/dt to be measured and the sensor's response and rise time, maximum possible di/dt overloads to be withstood by the sensor but not to be measured, maximum sensor recovery time after di/dt overload
	dv/dt	Maximum error allowed during dv/dt, maximum settling time of sensor after dv/dt disturbance
	Frequency range	Harmonic content, frequency range to be measured, fundamental operating frequency
Mechanical interfaces	External dimensions	Aperture location, connector location, required clearance distances, maximum specified dimensions
	Primary electrical connection	Printed circuit board (PCB) pins, busbar dimensions, aperture size and shape, other connections
	Secondary electrical connection	PCB pins, screw lugs, fasten tabs, connector, other connections
	Package fastening	PCB mount, aperture mount, rail mount, panel mount

1.6. LOCATIONS FOR SENSING CURRENT

Several possible current sensing locations in a power electronic converter are shown in Figure 1.1 [38]. The current sensing locations are selected based on the desired information and on which circuit branch it is available.
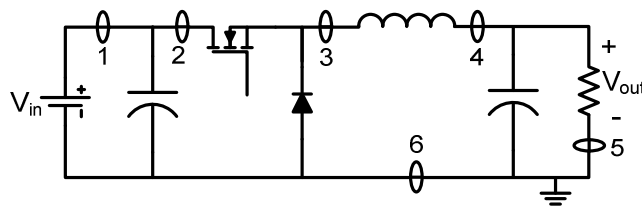
Figure 1.1. Possible current sensing locations in typical power switching stage

Sensing location 1 is good for sensing total input current (dc and ripple), which is required for power factor control, short circuit protection, and input power calculations. Sensing location 2 measures the switch current. It is a good location for peak current-mode control and overall short circuit protection. Sensing location 3 gives average current information. This location is not effective due to the wide voltage swing. Sensing location 4 gives information about both instantaneous inductor current and average load current, which are useful for average current-mode control. Sensing at location 5 is easier than all of the locations discussed above. This location yields true information about the output current. However, this information is not useful for short circuit protection. Grounding will affect the regulation at this location because the voltage across sensing element needs to be subtracted from the output voltage V_{out}. The problem with location 6 is the separation of load grounding from the input.

In motor drives systems, protection and control are implemented by measuring the current at different positions, as shown in Figure 1.2. Sensing location 1 protects the motor inverter by measuring the input current. Sensing location 2 protects the semiconductors by direct current measurement. Sensing location 3 effectively senses the motor current as a part of the speed control system. Sensing location 4 detects the dc link current and polarity to protect semiconductor devices.
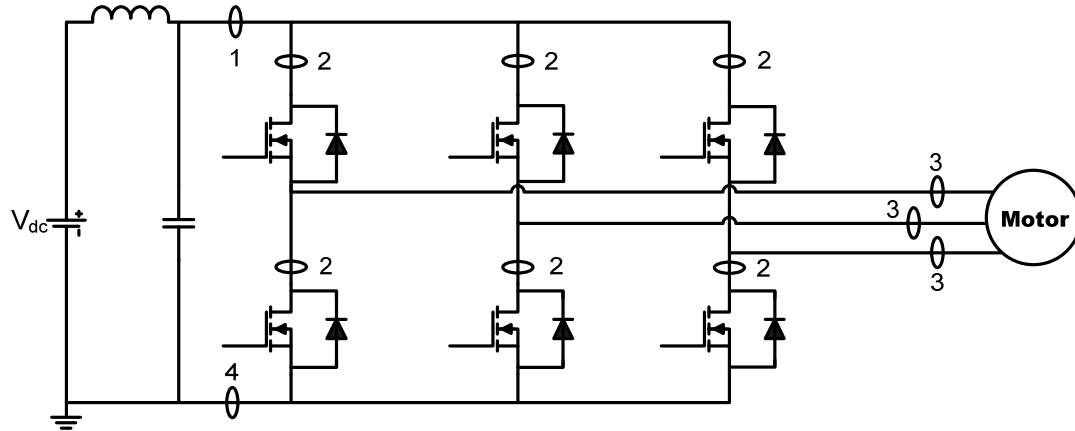
Figure 1.2. Possible current sensing locations in motor drives

1.7. THESIS ORGANIZATION

In this thesis, several current sensing techniques have been reviewed and evaluated which are different in accuracy, complexity, cost, operating range, linearity, current magnitude, bandwidth, electric isolation, switching noise sensitivity, and ac response. Different resistive-based current sensing methods are presented in Section 2. Section 3 discusses various electromagnetic-based current sensing techniques. Section 4 provides information about different current sensing techniques with self-tuning and/or self-calibration. Average current sensing techniques are discussed in Section 5. At the end of each Section, all of the current sensing techniques presented in the Section are compared. Finally, Section 6 presents an overall evaluation of current sensing techniques.

2. RESISTIVE-BASED CURRENT SENSING TECHNIQUES

According to Ohm's law, when current is flowing through a resistor, there is a voltage drop across it. Therefore, a resistor can be used to measure the current in a circuit and translate it into a voltage. This voltage signal is a representation of the current, which can be easily measured and monitored by control circuitry. The sense resistor, the resistor used for current measurement, must have low resistance to minimize its power consumption [39].

2.1. RESISTIVE-BASED CURRENT SENSING TECHNIQUE USING AN EXTERNALLY ADDED SENSE RESISTOR

A current detecting circuit of a dc-dc converter using an external sense resistor R_{sense} is shown in Figure 2.1. R_{sense} acts as a current to voltage converter.
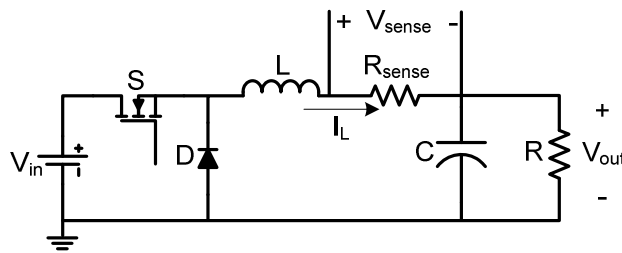
Figure 2.1. Current sensing using an externally added sense resistor

Discrete resistor and PCB trace are the most common types of R_{sense} [40-44]. If R_{sense} value has tight tolerance, this technique is accurate for low current values. When resistor R_{sense} is crossed by inductor current I_L in a buck converter, current I_L is sensed by

measuring the voltage (V_{sense}) across sense resistor R_{sense}, as depicted in Figure 2.1. Current I_L is given by (2.1).

$$I_L = \frac{V_{sense}}{R_{sense}} \qquad\qquad (2.1)$$

Due to its simplicity and accuracy, this method is used for power factor correction and over current protection. The criteria for the selection of R_{sense} are voltage drop, accuracy, efficiency and power dissipation, parasitic inductance, and cost. The drawback of this technique is the power loss incurred by resistor R_{sense}. Therefore, this method is inefficient for dc-dc converters. Additionally, it does not provide measurement isolation from transient voltage potentials on the load. A noise filter is required to reduce the noise in the signal output, which will affect the overall system bandwidth. This technique is not applicable to high performance dc-dc converters whose efficiency requirements are more than 85-90%.

If resistor R_{sense} is placed on the load side (see Figure 2.1), it only gives information about the output current. Input current measurement is required to achieve adaptive voltage positioning in voltage regulators. Input current sensing is achieved by placing R_{sense} on the input side. A modified metal oxide semiconductor (MOS) current sensing technique using a current mirror to overcome power loss incurred by sense resistor is presented in [45]. This method measures the current without requiring the entire output current to pass from the series sense resistor. This technique uses the microelectronic current mirroring concept. The current passing through the sense resistor is proportional to the output current and its magnitude is smaller.

2.2. RESISTIVE-BASED CURRENT SENSING TECHNIQUE USING THE INTERNAL RESISTANCE OF AN INDUCTOR

To avoid the use of sense resistor and to reduce the power loss it creates, an inductor is used for current sensing, as depicted in Figure 2.2 [38]. This method is appropriate for low voltage power converters. Resistor R_L in series with inductor L is the internal resistance or direct current resistance (DCR) of the inductor winding.
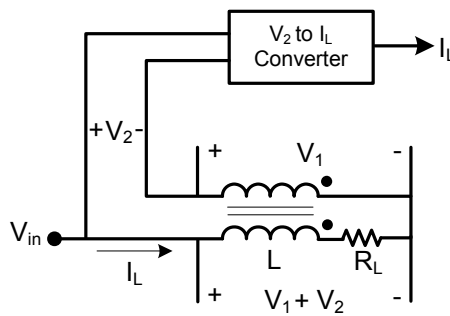
Figure 2.2. Current sensing using the internal resistance of an inductor

The voltage across the main inductor is made of two voltages V_1 and V_2, which are given by (2.2).

$$V_L = V_1 + V_2 = L\frac{dI_L}{dt} + I_L R_L \tag{2.2}$$

An extra winding with an equal number of turns and minimum current loading is coupled with the main inductor, as shown in Figure 2.2. The voltage across the extra winding is V_1 due to the equal number of turns. If the voltages of both windings are added, the resulting voltage is simply $I_L R_L$ drop. The disadvantage of this technique is that the measured current is inaccurate because V_2 which is the difference between two

large voltages is quite small. Inductor winding is built by copper wire, so, the temperature coefficient of copper's resistivity also applies.

2.3. MOSFET R$_{DS}$-BASED CURRENT SENSING TECHNIQUE

A lossless MOSFET drain-source resistor-based current sensing method, which eliminates the need for resistor R$_{sense}$ for current sensing, is depicted in Figure 2.3 [46-49]. The drain-source resistance (R$_{DS}$) of the MOSFET is useful for current measurements. A MOSFET acts like a resistor when it is on, so it is possible to determine current I$_L$ by measuring the drain-source voltage of the switch.
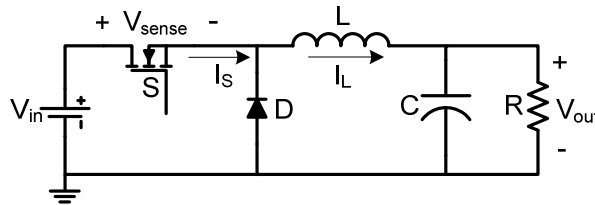
Figure 2.3. MOSFET R$_{DS}$-based current sensing

Current I$_L$ can be determined by measuring switch current I$_S$. As switch S is on in a buck converter during the time interval 0<t<dT only, a sample-and-hold circuit is required to sense current I$_L$. Current I$_S$ is determined by measuring the voltage across resistor R$_{DS}$. Current I$_S$ is given by (2.3).

$$I_S = I_L = \frac{V_{sense}}{R_{DS}}$$

(2.3)

A MOSFET is in the triode region when it is conducting and voltage across it is low. MOSFET acts like a resistor in this case. The resistance R_{DS} is given by (2.4).

$$R_{DS} = \frac{L}{W\mu C_{OX}(V_{in} - V_T)}$$ (2.4)

Where μ is the electron mobility, C_{ox} is the oxide capacitance, and V_T is the threshold voltage. The value of resistance R_{DS} is given in the MOSFET data sheet. The accuracy of this method depends on the tolerance of resistor R_{DS}. The datasheet gives only the maximum and typical values of resistor R_{DS}, not the minimum.

MOSFET R_{DS}-based current sensing is a very low cost method for current sensing. One of the uses of this method is in low-voltage, high-current point of load converter applications. However, the actual current threshold will vary with resistance R_{DS}. Resistance R_{DS} varies with temperature, gate drive voltage, and individual devices. Variations in the gate drive amplitude result in a poor current sensing accuracy in multiphase converters. Higher switching frequencies and higher input voltages make this method complicated.

2.4. CURRENT-SENSING POWER MOSFET-BASED CURRENT SENSING TECHNIQUE

Current-sensing power MOSFET technique is more accurate than the MOSFET R_{DS}-based current sensing technique [50-57]. A power MOSFET consists of a large number of parallel connected MOSFET cells. The gates, sources, and drains of all transistor cells are connected together. However, when power MOSFET is tuned on to sense the current, the entire amount of the sense current passes through sense resistor, so there is a significant and undesirable power loss. To avoid this power loss, few cells in

the power MOSFET are utilized to provide sensing FET (SENSEFET). Remaining transistor cells are used to provide the switching MOSFET. This new power MOSFET structure is known as a current-sensing power MOSFET. The current-sensing power MOSFET is a parallel connection of a SENSEFET (S_2) and switching MOSFET (S_1), as shown in Figure 2.4. Switch S_2 has relatively fewer transistor cells to provide a small sensing signal proportional to the switch S_1 current. A sense resistor is placed on the scaled down current to reduce the power dissipation; therefore, this technique is used to provide accurate and lossless current measurement. A current-sensing power MOSFET is symbolically represented in Figure 2.4.
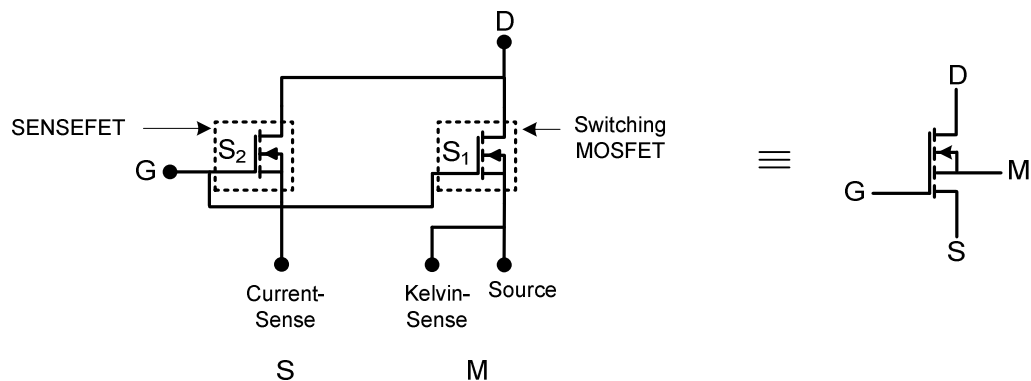
Figure 2.4. Current-sensing power MOSFET

The current-sensing power MOSFET is a five terminal device. Switches S_1 and S_2 have identical unit cell structures and reside on the same silicon substrate. Their gate terminals are connected to a common terminal G and their drain terminals are connected to a common terminal D. Source terminals of switch S_2 are connected to a current sense or mirror terminal S and source terminals of switch S_1 are connected to a main terminal

M which consists of Kelvin-sense terminal K and source terminal S. A Kelvin-sense terminal is shorted internally to the source terminal of switch S_1 to bypass the packaging and interconnection parasitic resistance associated with switch S_1. It provides more accurate current sensing.

The most common practice of using S_1 and S_2 for current sensing in a buck converter is shown in Figure 2.5. N is a predetermined ratio of the transistor cells of switch S_1 to switch S_2. For example, N may be in the order of 100 to 1000. If N increases, accuracy of the circuit decreases. All transistor cells of the current-sensing power MOSFET are similar; therefore, if the sources of switches S_1 and S_2 are virtually connected, switches S_1 and S_2 pass currents in the ratio N:1, and have resistances in ratio 1:N.
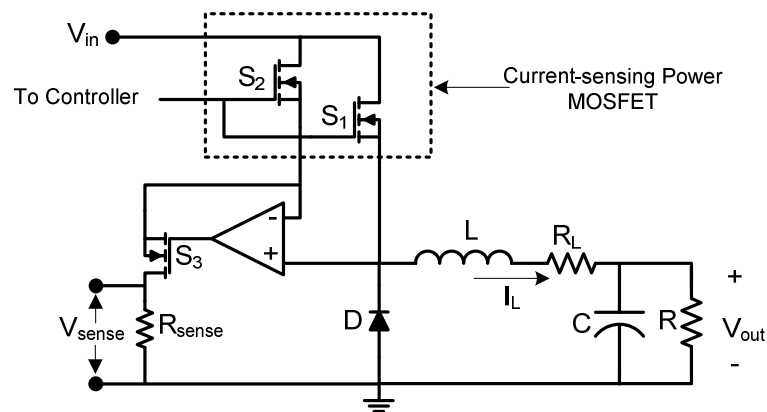
Figure 2.5. Current-sensing power MOSFET-based current sensing

An operational amplifier in Figure 2.5 is used to make the gate-to-source voltages of both switches equal. Since only a predetermined fraction of total current is passing

through R_{sense}, power dissipation in R_{sense} is low. As current passing through S_1 is not continuous, a sample-and-hold circuit holds the sensed current when S_1 is off. The sense voltage V_{sense} in this technique is given by (2.5).

$$V_{sense} = R_{sense} \left(\frac{I_L}{N} \right)$$
(2.5)

The use of current-sensing power MOSFET is impeded by its limited availability and high cost. This method is not applicable to high frequency systems because it introduces switching transients and noise to the sense signal. The accuracy of this method is limited because it works only when switches S_1 and S_2 are matched. Because this technique's current ratio is N:1, a low degree of coupling between S_1 and S_2 can induce a significant error and large spikes are injected in the sense signal during high di/dt periods.

2.5. PWM-VSI SWITCHING STRATEGIES

For the purpose of motor current sensing, the switching strategies of an inverter are discussed in this sub-section, assuming its load is a three phase star connected motor. However, the same reasoning is applied to single phase or poly-phase and star or delta connected synchronous or asynchronous motors.

PWM techniques are used in voltage source inverters (VSI) to control different types of motors. A three phase PWM-VSI driven ac motor is depicted in Figure 2.6. All three legs of an inverter are supplied by a dc voltage source. A large capacitor connected at the input terminals tends to make the input dc voltage constant and suppresses the harmonic fed back to the source. A control signal is provided through the gate of each transistor.
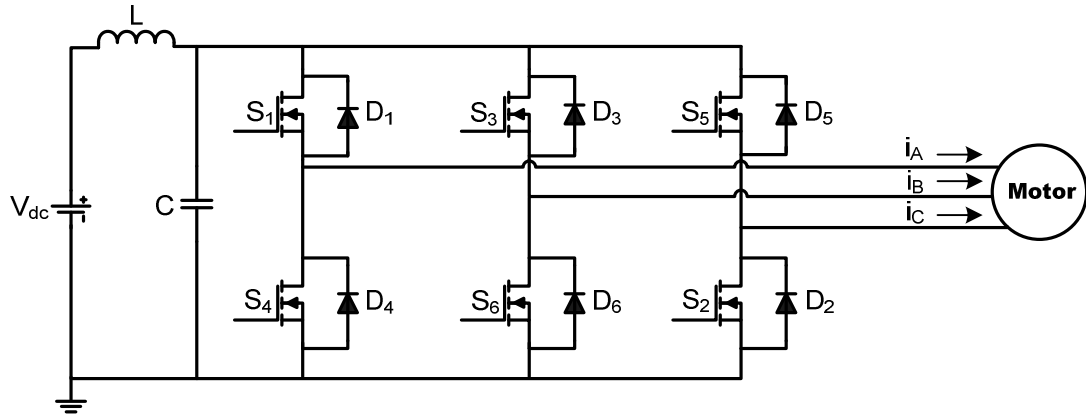
Figure 2.6. PWM-VSI driven ac motor

Switches in VSI are numbered in the sequence in which they are triggered. Three phase VSI works with either 180° or 120° conduction mode [58, 59].

If three phase VSI works with 180° conduction mode, switch pairs S_1, S_4; S_3, S_6; and S_5, S_2 are turned on with a time interval of 180°, which means S_1 conducts for the first 180° and S_4 for the next 180° of a cycle, as shown in Figure 2.7.
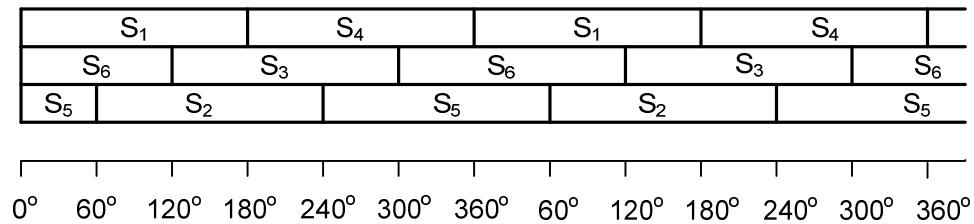
Figure 2.7. Switching sequence of a 180° VSI conduction

Switches in the upper group, i.e, S_1, S_3, and S_5, conduct at an interval of 120°, which implies that if S_1 is fired at angle 0°, then S_3 must be fired at angle 120° and S_5 at

angle 240° [59]. Each arm of a three phase VSI has three possible states, so a total of twenty-seven combinations are possible. Only eight states that do not involve both transistors of any phase to be on at once are used. During remaining nineteen states the phase voltage depends on the conduction of freewheeling diodes. Eight different states of six switches are given in Table 2.1 for 180° VSI conduction. A simple logic circuit is required to identify states 1-6 of Table 2.1. Control signals are then fed to the inverter. However, control signals provided to the upper legs of inverter are opposite to the control signals provided to the lower legs.

Table 2.1. Different states of a 180° VSI conduction

State	S_1	S_2	S_3	S_4	S_5	S_6
0	off	on	off	on	off	on
1	on	off	off	off	on	on
2	on	on	off	off	off	on
3	on	on	on	off	off	off
4	off	on	on	on	off	off
5	off	off	on	on	on	off
6	off	off	off	on	on	on
7	on	off	on	off	on	off

If three phase VSI works with 120° conduction mode, each switch conducts for 120° of a cycle, as shown in Figure 2.8. Like 180° mode, 120° mode VSI also requires six steps, each of 60° duration, to complete one cycle of the output ac voltage. The six different possible states of six switches are given in Table 2.2 for 120° VSI conduction.
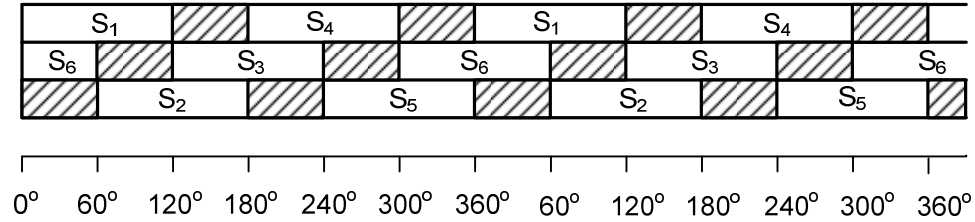
Figure 2.8. Switching sequence of a 120° VSI conduction

Table 2.2. Different states of a 120° VSI conduction

State	S_1	S_2	S_3	S_4	S_5	S_6
1	on	off	off	off	off	on
2	on	on	off	off	off	off
3	off	on	on	off	off	off
4	off	off	on	on	off	off
5	off	off	off	on	on	off
6	off	off	off	off	on	on

2.6. CURRENT SENSING TECHNIQUES FOR PWM-VSI DRIVEN AC MOTOR USING EXTERNALLY ADDED SENSE RESISTORS

Different current sensing strategies for measuring motor current using externally added sense resistors are described in this sub-section.

2.6.1. An Externally Added Sense Resistor in Each Leg of the Inverter. For certain applications, the current must be measured in individual legs of the motor controller inverter for various purposes. A VSI with current sensors in the three low side inverter switches to achieve closed-loop current regulation is shown in Figure 2.9. Sense resistors are used to sense the current flowing through each leg of the motor controller circuit [60-62]. Sense resistors are connected to the source pin of each low side transistor.
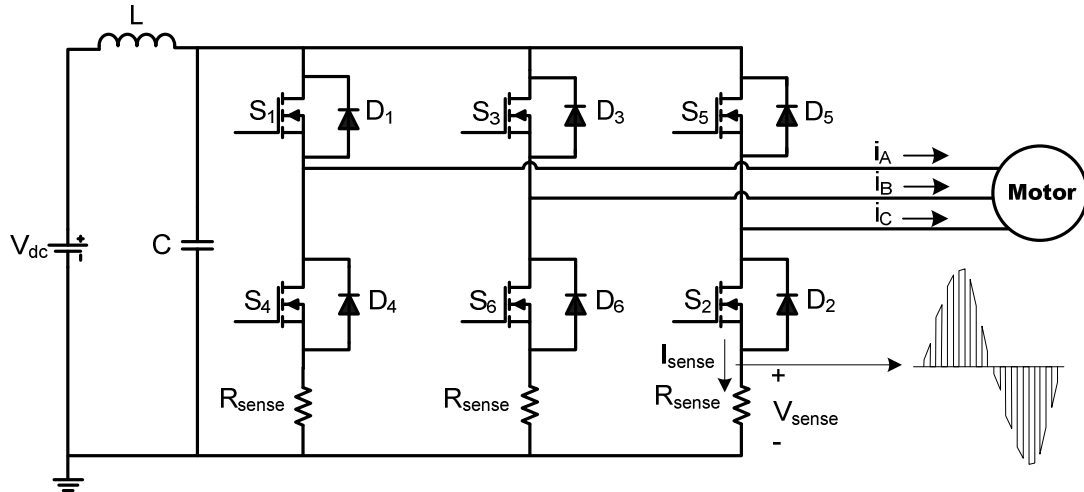
Figure 2.9. Motor current measurement using an externally added sense resistor in each leg of VSI

When VSI operates with 180° conduction, at any given instant of time all three motor phases carry currents. Therefore, when two lower leg switches are on, two of the three motor phase currents are determined by measuring the voltages developed across R_{sense} (V_{sense}) to obtain complete motor line current information. For instance, if switches S_1, S_6, and S_2 are on, voltages developed across resistors R_{sense} are measured to determine currents i_B and i_C. Using the information about currents i_B and i_C, it is easy to calculate current i_A. However, the current measured by this technique is the half bridge current not the motor phase current, as shown in Figure 2.9. Sample-and-hold circuit is required to reconstruct the motor phase current.

In order to get a good sample of voltage V_{sense} for current measurement, the width of lower leg pulse must be long enough. However, if lower transistors are turned on for a high portion of PWM period, it will create noise problems for the entire sense output sampling circuit due to high dv/dt and di/dt.

2.6.2. Externally Added Sense Resistors in Series with Motor Phases. In this method, the sense resistors are connected in series with motor phases, as depicted in Figure 2.10 [63, 64]. The voltage drop across each resistor is measured to determine the current flowing through each phase. Also, at any given instant of time in this method, only two phase currents need to be measured to get full information about motor line currents.
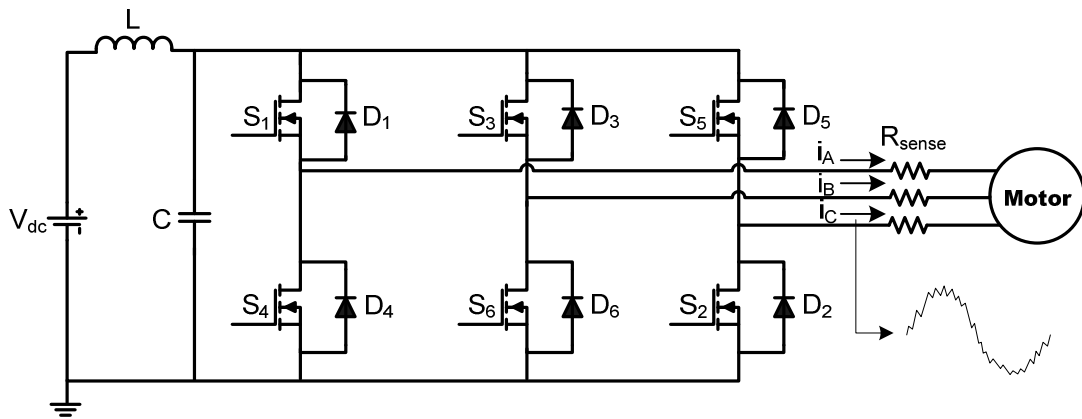
Figure 2.10. Motor current sensing using externally added line sense resistors

This method's major disadvantage is that the measured current has a common mode rejection problem because the small common mode signal with fast dv/dt rides on top of the measured current, as shown in Figure 2.10. A common method of solving the common mode rejection problem is to use an optically coupled isolated amplifier. However, if resistance is small when measuring higher currents, the inductive component of the impedance begins to dominate.

2.6.3. An Externally Added Sense Resistor with DC Link. Depending on the states of transistor switches and period of operation, the current through the motor phases can be measured or calculated by a single resistor, as shown in Figure 2.11. In the dc link sense resistor method, a single resistor is placed on the dc link between the dc power supply and the inverter to avoid level shifting during current measurement [65-78]. The dc link sense resistor minimizes the cost and power dissipation.
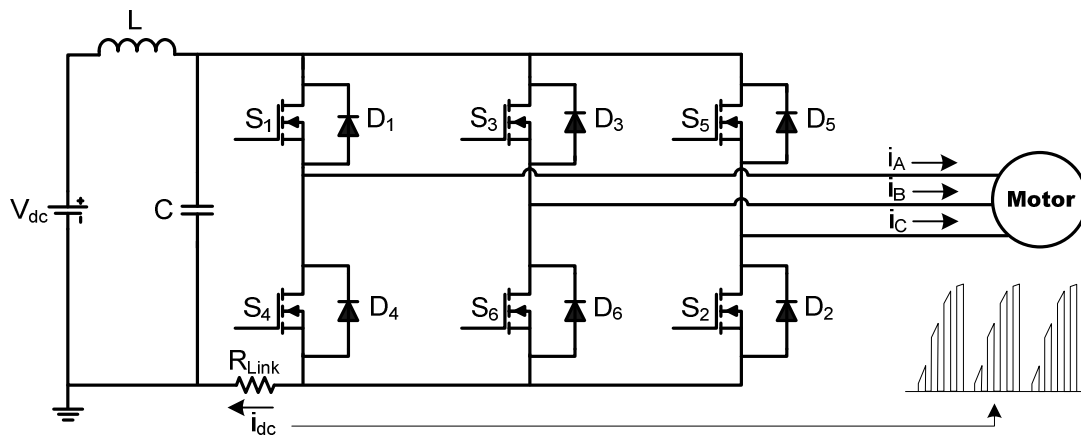
Figure 2.11. DC link current sensing using an externally added sense resistor

In ac drive systems, as mentioned earlier, if VSI works with 180° conduction, current I_{dc} is equal to one of the motor phase current or opposite to it for six different states, as depicted in Table 2.3. I_{dc} is zero when the upper three switches are on and the lower three switches are off or vice versa. If VSI works with 120° conduction, at any given instant the phase currents are expected to flow in only two phase windings (the third phase current is zero). Only one current measurement is necessary in the dc link and

other phase motor current can be reconstructed from dc link current information as depicted in Table 2.3.

It is also possible that the machine winding currents circulate within the VSI with some switching strategies, so there is no current available in the dc link for measurement. Furthermore, the measured current is the total bus current, not the phase current, as shown in Figure 2.11. The phase currents are reconstructed using measured dc link current and the knowledge of the switching states [78].

Table 2.3. DC link current for a PWM-VSI driven motor with 180° and 120° conduction

State	i_{dc} for 180° Conduction	i_{dc} for 120° Conduction
1	$-i_B$	$i_A = -i_B$
2	i_A	$i_A = -i_C$
3	$-i_C$	$i_B = -i_C$
4	i_B	$i_B = -i_A$
5	$-i_A$	$i_C = -i_A$
6	i_C	$i_C = -i_B$

No switch status information is needed in the inverter for current measurement if the sense resistor is connected to the positive rail of the VSI. However, the inverter circuit becomes more complicated to avoid reverse current flow into the sense resistor. The voltage information at two points of R_{sense} is required to find the voltage drop across R_{sense} in this method, whereas voltage measurement at only one point is required when R_{sense} is connected to the negative rail. It is also possible to connect the dc link sense resistor between the dc source and the capacitor, rather than between the capacitor and the inverter on the negative rail.

2.7. MOSFET R_{DS}-BASED CURRENT SENSING FOR PWM-VSI DRIVEN AC MOTOR

A MOSFET switch has a linear resistance characteristic when it is on. Therefore, when the MOSFET switch is on in VSI, it is possible to get the motor current information from voltage drop observed across it. The circuit used to sense the single motor phase current by measuring the low side MOSFET switch (S_4) voltage is depicted in Figure 2.12 [79]. The other two phases are exactly the same.
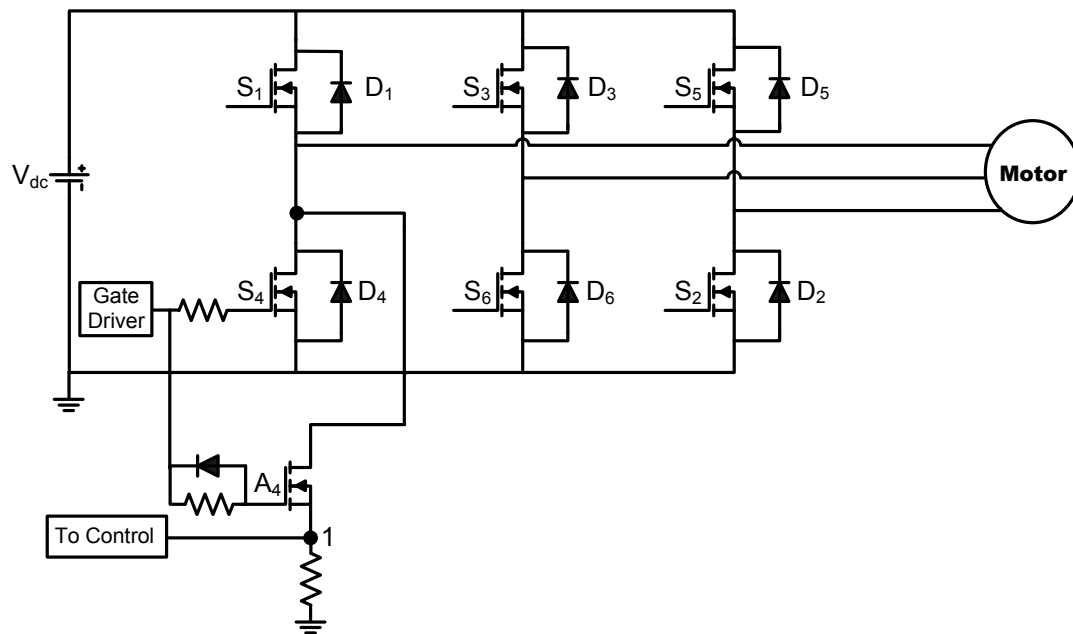
Figure 2.12. MOSFET R_{DS}-based current sensing technique for motor current detection

When low side MOSFET switch S_4 is on, switch A_4 also turns on, and the voltage at point 1 is the same as the voltage drop across switch S_4. When MOSFET switch S_4 is off, switch A_4 also turns off, and the voltage at point 1 is zero. If the voltage drop at point 1 and resistance R_{DS} of switch S_4 are known, it is easy to derive the motor phase current

passing through switch S_4. The current information obtained from this technique is useful for current protection purposes; hence variation in R_{DS} is acceptable.

2.8. CURRENT-SENSING POWER MOSFET-BASED CURRENT SENSING TECHNIQUE FOR PWM-VSI DRIVEN AC MOTOR

A technique for phase current measurement in VSI using current-sensing power MOSFET is depicted in Figure 2.13 [80-88]. In this method each of the three lower leg MOSFET switches in VSI are replaced by current-sensing power MOSFETs. Current-sensing power MOSFET enables accurate and low cost current measurement. These current sensors are designed to accurately mirror the motor phase current.
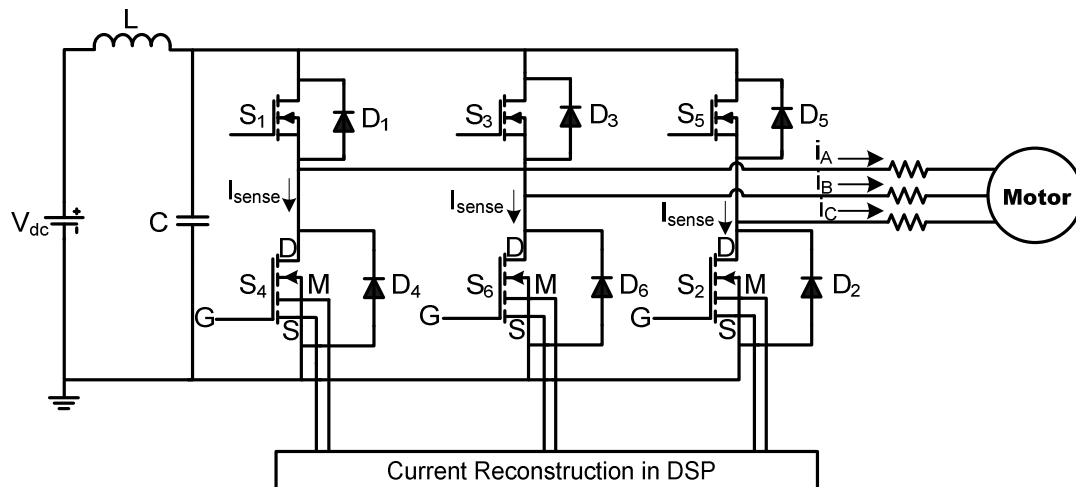
Figure 2.13. Current-sensing power MOSFET-based current sensing technique for motor current detection

A limitation of this technique is that its ability to measure the current only when the current flowing through it is in a forward direction, which is only possible when the polarity of the phase current is negative. Another limitation is that, at each particular

instant, two lower leg switches need to be on for complete current measurement. However, the current measurements taken using this technique are incomplete because the output phase current passes through the low side switch for only half of the fundamental cycle. Therefore, the alternating 60° intervals (three times during each fundamental frequency cycle) provide incomplete current information. A technique is depicted in [82] to reconstruct the three phase currents during the intervals when they are not measured.

It is also possible to connect the current sensors to the upper leg of VSI, but it requires high performance level shifting to transfer the sensed signal to a common reference. On the contrary, if the current sensors are in the lower leg of VSI, they can share the same reference terminal, simplifying the signal conditioning.

2.9. COMPARISION BETWEEN RESISTIVE-BASED CURRENT SENSING TECHNIQUES

Table 2.4 summarizes the advantages and disadvantages of the presented resistive-based current sensing techniques.

Table 2.4. Comparative overview of resistive-based current sensing techniques

Techniques	Advantages	Disadvantages
Using an externally added resistor	Simple, accurate, low cost	Power loss incurred by sense resistor
Using the internal resistance of an inductor	Accurate, lossless	Not useful for high power applications
MOS current sensing	Lossless, accurate	Complicated circuit, accuracy depends on matching performance of the current mirror
Using the internal resistance of a MOSFET	Lossless, no additional sensing component required, low cost	Not accurate for high input voltage and high switching frequency, affected by temperature variations of R_{DS}, discontinuous and noisy
Using current-sensing power MOSFET	Lossless, practical, accurate with respect to temperature variations, no additional sensing component required, low cost	Special MOSFET, introduce switching transients and noise at high frequency, accuracy depends on matching performance of the current mirror, switching noise, limited applications, discontinuous and noisy

3. ELECTROMAGNETIC-BASED CURRENT SENSING TECHNIQUES

Resistive-based current sensors are acceptable where power loss, low bandwidth, noise, and non isolated measurement are acceptable. These sensors are not used in high power applications where isolation is required. Solution to these problems is electromagnetic-based current sensing techniques.

Based on Ampere's law, the current flowing through a conductor generates magnetic field. Hence, sensing the magnetic field surrounding a conductor provides information about its current. Electromagnetic-based techniques work based on this phenomenon while they provide galvanic isolation between the control and power stages, higher bandwidth, and lower power losses. The lower power dissipation of electromagnetic-based current sensors allow much higher signal level, significantly improves the signal-to-noise environment of the control system [39].

3.1. CURRENT MEASUREMENT TECHNIQUES USING CURRENT TRANSFORMERS

A current transformer (CT) is similar to a voltage transformer; except that the primary input is a current. There are four basic types of CTs [89-92]: ac current transformers (ACCTs), unidirectional current transformers (UCTs), dc current transformers (DCCTs), and fly-back type current transformers (FBCTs). ACCTs and UCTs are commonly used, DCCTs are used for high current applications, and FBCTs are used when current pulses are very short.

CTs are used with low range ammeters to measure currents in high voltage circuits. In addition to providing insulation from the high voltage side, CTs step down the

current in a known ratio. Their physical basis is the mutual induction between two circuits linked by a common magnetic flux. A CT consists of two inductive coils, which are electrically separated but magnetically linked through a path of low reluctance, as shown in Figure 3.1. If one coil is connected to an ac source, an alternating flux is set up in the core, most of which is linked with the other coil in which it produces mutually induced electromotive force (EMF) according to Faraday's law of electromagnetic induction. The first coil is called the primary coil, and second coil is called the secondary coil of the CT. If the secondary of the CT is closed, electric energy is magnetically transferred from primary to secondary.
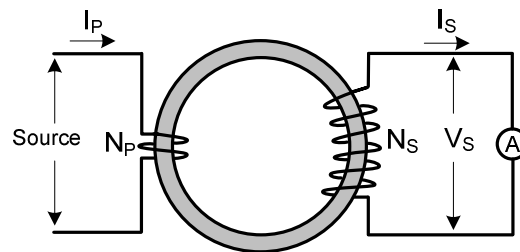
Figure 3.1. Current transformer

For an ideal transformer with no load, the induced secondary EMF is same as the secondary terminal voltage (V_S). The relationship between the primary and secondary voltages, currents, and number of turns is given by (3.1).

$$\frac{V_P}{V_S} = \frac{I_S}{I_P} = \frac{N_P}{N_S} \tag{3.1}$$

Where V_P and V_S are primary and secondary terminal voltages, I_P and I_S are primary and secondary winding currents, and N_P and N_S are the number of primary and secondary turns, respectively.

For typical switching converter applications, a CT has single turn primary and multi-turn secondary. The basic CT schematic is given in Figure 3.2.
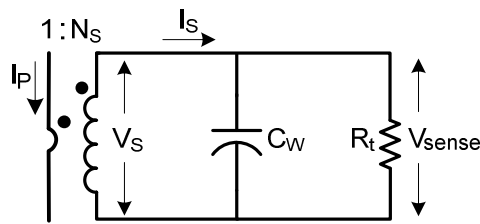
Figure 3.2. Basic circuit of single turn primary current transformer

The primary is formed by wire from which an unknown current is passing. The secondary has large number of turns and it is terminated by terminating or burden resistor (R_t). If the number of secondary turns is too large, then there will be a significant inter-winding capacitance (C_W). In addition to primary and secondary windings, capacitance C_W is also added in the model of a CT.

The relationship between currents I_P and I_S in this case is given by (3.2).

$$\frac{I_S}{I_P} = \frac{1}{N_S}$$

(3.2)

Capacitor C_W is not considered here since the measured frequency is low. The secondary output voltage (V_{sense}) in a CT is proportional to the resistor R_t based on the current flowing through it. Voltage V_{sense} across the secondary is given by (3.3).

$$V_{sense} = I_S R_t = \frac{I_P}{N_S} R_t \qquad (3.3)$$

One of the most commonly used CTs is known as clamp-on or clip-on type. It has a laminated core which is arranged in such a manner that it can be opened by pressing a switch, permitting the admission of the current carrying conductor. The current carrying conductor acts as a single turn primary, whereas secondary is connected across the standard ammeter.

CTs are used in control and limiting applications. The advantages of a CT include good signal-to-noise ratio (SNR), galvanic isolation between control circuit and the line being monitored, good common mode rejection, high bandwidth (50 or 60 Hz to 20 kHz), and low power loss in high-current applications. Galvanic isolation is required to protect the sensing device from high power signals and to reduce the power dissipated by the sensing resistor. The secondary side current can be made smaller by using a larger turns ratio. CTs are relatively simple to implement and are passive devices that do not require driving circuitry for operation. The major disadvantages of CTs are their higher cost, larger size, and non-integrality. An ACCT gets saturated if input is direct current. Yet, some methods are used to sense the switch dc current in switching power converter using CTs. It is due to the fact that switch currents in the converter are interrupting, allowing time for transformer reset.

3.1.1. Using the Existing Inductor as the Primary of a Transformer. This technique measures the current flowing through an inductor by using existing inductor of a converter as the primary of a transformer. Primary current I_L will generate magnetic field that is coupled into a secondary coil. As shown in Figure 3.3, in a buck converter, the inductor is used as the primary side of a transformer, and the secondary side develops voltage proportional to current I_L [42].
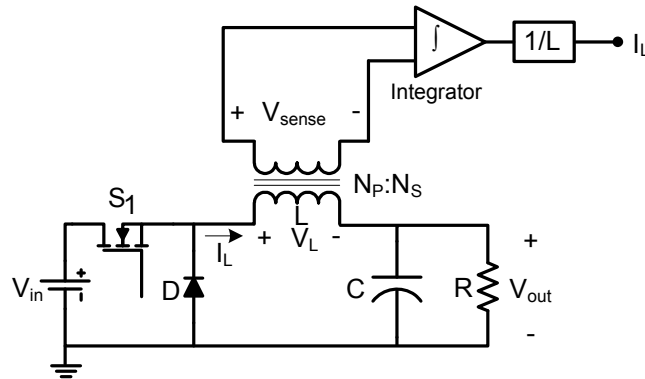
Figure 3.3. Current measurement using the existing inductor as the primary of a transformer

Inductor current in this technique is calculated by (3.4). For integration it is necessary to know the value of inductance L.

$$i_L = \frac{1}{L} \int v_{sense} dt \qquad (3.4)$$

This technique measures the fraction of the high inductor current. The transformer only passes the ac part of current I_L, not the dc, and no information about average current is provided by technique. This technique is not appropriate for over current protection.

The presence of the dc current affects the low frequency performance of ACCT. In order to recover the dc component of the current signal during current measurement, the following techniques are used.

3.1.2. AC Current Transformer with Sample-and-Hold Circuit. The magnetic core of the ACCT needs to be optimized such that the ACCT is able to function with a primary current having a dc current component. One method of gathering full information about current I_L in the buck converter is depicted in Figure 3.4 [93]. Two ACCTs, CT_1 and CT_2, are used to measure the two switch currents. Additional circuits are required to reconstruct the two switch current signals. Reconstructed current outputs of CT_1 and CT_2 are then added to obtain full information about current I_L. Two blocks with gain $N_P/(N_S R_t)$ are required to adjust the different scaling used in the two CTs.
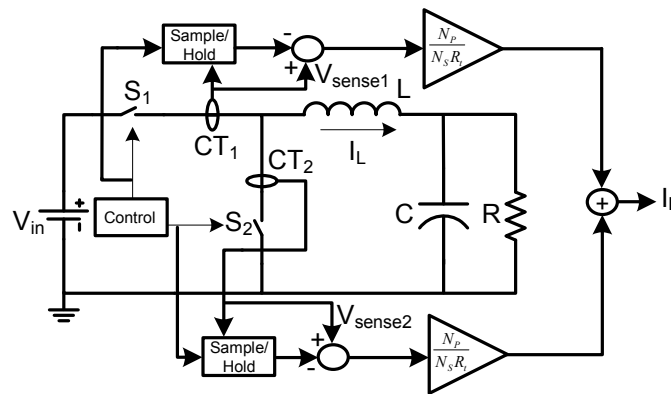
Figure 3.4. Inductor current estimation using two ac current transformers

Usually, CT_1 and CT_2 will filter off the dc component of the primary current, so they allow only the ac part on the secondary side. In order to obtain full information of current I_L, additional sample-and-hold circuits are required for switch current

reconstruction, as depicted in Figure 3.4. Current sensor waveforms for CT_1 are shown in Figure 3.5.
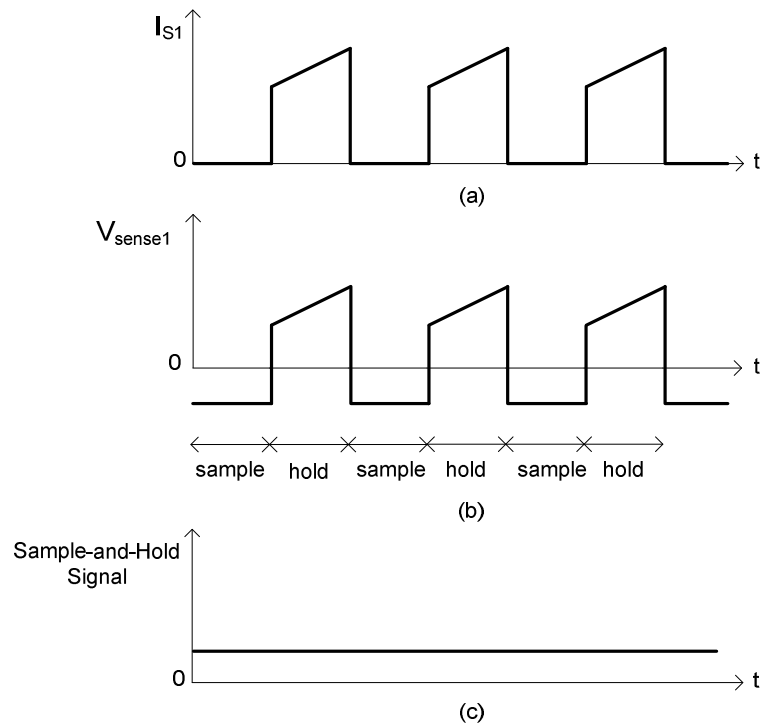
Figure 3.5. Current, voltage, and sample-and-hold circuit waveforms for CT_1

Figure 3.5 (a) shows the ideal switch current (I_{S1}) waveform for switch S_1. The dc component of current I_{S1} is filtered off in the secondary voltage (V_{sense1}) of CT_1 as shown in Figure 3.5 (b). However, no information is lost in this process. In order to obtain complete inductor current information in each cycle, sample the value of voltage V_{sense1} when switch S_1 is turned off, hold that value when switch S_1 is turned on, as shown in Figure 3.5 (c). The output of the sample-and-hold circuit is deducted from the voltage V_{sense1} to get a signal which is proportional to current I_{S1}. Current through switch S_2

(I_{sense2}) is estimated in the same manner as with switch S_1. Two switch current signals are added to estimate I_L. High bandwidth sample-and-hold IC is required in this method.

There are some design requirements for the ACCT core in this method. For CT, if H is the magnetic field intensity and l is the magnetic mean path, then according to Ampere's law, the magneto-motive force (MMF) is given by (3.5).

$$N_P I_P + N_S I_S = Hl \tag{3.5}$$

If ϕ is the total flux, B is flux density, A is the cross sectional area of the core, μ_o is the vacuum permeability, μ_r is the relative permeability, and R_e is the reluctance of the magnetic circuit, (3.5) can be rewritten as (3.6).

$$N_P I_P + N_S I_S = \frac{B}{\mu_0 \mu_r} l = \frac{\phi}{\mu_0 \mu_r A} l = R_e \phi \tag{3.6}$$

According to Faraday's law of electromagnetic induction, the secondary voltage is given by (3.7).

$$V_{sense} = I_S R_t = N_S \frac{d\phi}{dt} \tag{3.7}$$

From (3.6) and (3.7), ratio of currents I_S and I_P is given by (3.8).

$$\frac{I_S}{I_P} = \frac{N_P}{N_S}\left(1 - \frac{1}{1 + ks}\right) \tag{3.8}$$

Where k is given by $(N_S{}^2)/(R_t R_e)$. Corner frequency (f_C) of low pass filter is specified by (3.9).

$$f_C = \frac{2\pi}{k} = \frac{2\pi R_t R_e}{N_S{}^2}$$ (3.9)

The first design requirement is that the f_C needs to be much lower than the switching frequency (f_S). The second design requirement is that the CT does not get saturated in its operation. More information about this requirement is discussed in detail in [3].

This technique has low power loss, fast response, and is accurate. It is also possible to obtain I_L by only measuring the high side switch S_1 current. A suitable analog circuit is required to connect the maximum and minimum points of the switch S_1 current to obtain full information about current I_L. The circuit required for that method is quite complicated.

3.1.3. Current Measurement using AC and Unidirectional Current Transformers. The magnetic flux in a typical ac transformer core alternates between positive and negative values, but not in the UCT. The UCT operates in a unipolar mode. For UCT, the core should have two properties; high permeability and low remanence.

The basic UCT circuit is shown in Figure 3.6 [94-97]. When a positive current pulse I_P flows in the primary of UCT, diode D conducts. Output voltage V_{sense} developed across resistor R_t is given by (3.3), and current I_S in this is given by (3.10).

$$I_S = \frac{I_P}{N_S} - I_M$$ (3.10)

Capacitor C_W is not considered here since frequency is low. Diode D will block the zero primary current and capacitor C will resonate with magnetizing inductor L_M to develop a negative half cycle sinusoidal pulse across secondary winding to reset the magnetizing current (I_M). Current I_M has a small value due to this cycle by cycle reset. This provides a fast reset for the transformer core, and isolates the negative reset voltage from the control circuit. Capacitor C_f is a filtering capacitor required for suppressing high frequency noise.
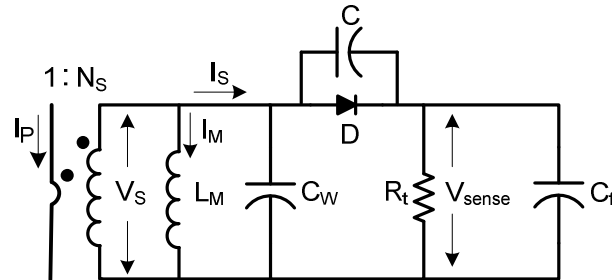
Figure 3.6. Basic circuit of a unidirectional current transformer

Waveforms for currents I_P and I_M and voltages V_S and V_{sense} of a UCT are given in Figure 3.7. During the pulse duration of current I_P, diode D conducts. The current I_S in R_t will be a transform of current I_P, and an analogue voltage of primary current will be developed across R_t. At the end of the conduction pulse, rapid UCT core recovery occurs because D blocks the reverse voltage across R_t. As a result, voltage V_S is large, enabling fast core restoration between pulses. For accurate current measurement by UCTs, inductance needs to be large to reduce current I_M. Current I_M increases during the pulse

duration. At the end of the conduction period, current I_M needs to be smaller than current I_P.
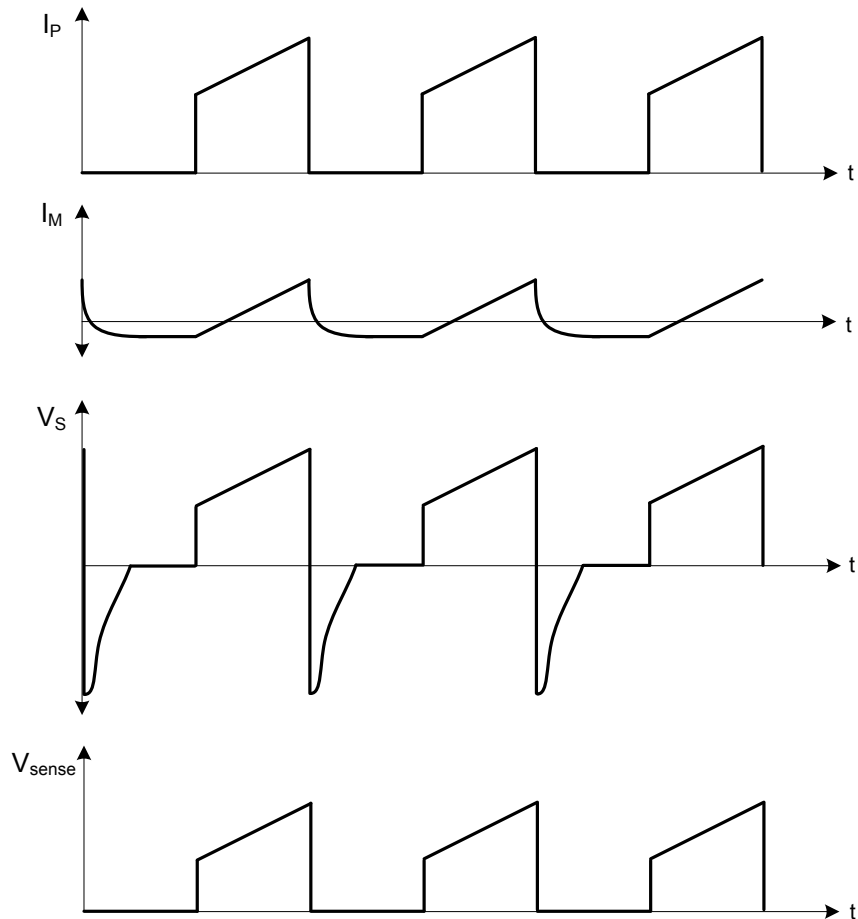
Figure 3.7. Unidirectional current transformer waveforms

A buck converter with UCTs and ACCT for current measurement is illustrated in Figure 3.8. The inductor current I_L and the output current I_O in any PWM converter are the combinations of the switch current I_S, the diode current I_D, and the capacitor current

I_C. These currents are ac or zero return pulse, which can be measured by using ACCTs and UCTs.
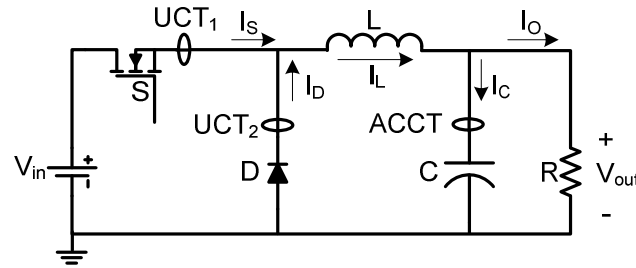
Figure 3.8. Current sensing using unidirectional and ac current transformers

In a buck converter I_L is given by (3.11).

$$I_L = I_S + I_D \tag{3.11}$$

UCT$_1$ and UCT$_2$ are used to measure I_S and I_D, as depicted in Figure 3.8. Current I_L is then derived from the information of the measured currents. Current I_C can be measured by using ACCT. Current I_O is derived from the information of currents I_L and I_C. In a buck converter, current I_O is given by (3.12).

$$I_O = I_L + I_C \tag{3.12}$$

This method is also useful for converters with isolation transformers. However, UCT has some limitations. There is no enough time for UCT to complete half cycle resonant reset at very high switching frequencies or very high or low duty cycles. The dc

magnetizing current in the transformer core will increase with a decrease in reset time. As a result, the dc level of the UCT output will drop.

3.1.4. DC Current Transformer. DCCT is used to accurately measure the dc current with low power loss. There are several different types of DCCT, one of which is shown in Figure 3.9 [98-100]. The secondary signal of DCCT is directly related to absolute value of primary current.
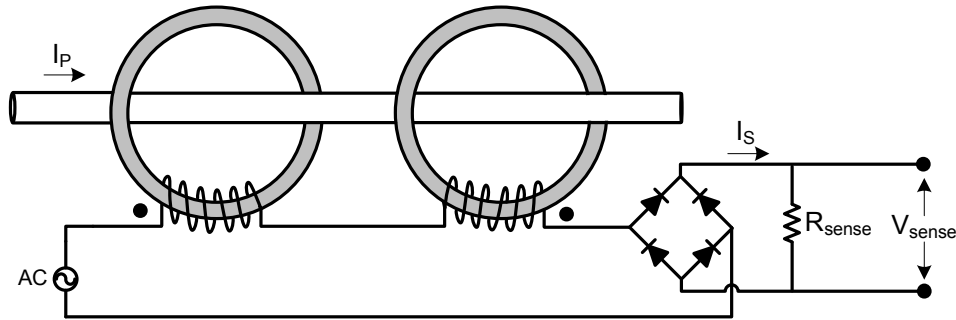
Figure 3.9. Current measurement using dc current transformer

DCCT has two ring cores, as depicted in Figure 3.9. AC supply is applied across their secondary to generate opposite polarity flux in each core, which will drive cores into and out of saturation. As each core comes out of saturation, the flux change induces a current I_S that is proportional to the current I_P. The rectifier is used to rectify the secondary signal. More information about this technique is given in [100].

3.2. CURRENT MEASUREMENT TECHNIQUES USING AIR CORE

The performance of a CT is often limited by the characteristics of its magnetic core material (hysteresis, non-linearity, losses, saturation, remanence (residual flux));

therefore, the design of an air core or coreless transformer is often considered. The challenge with air core current measurement techniques is to have enough measurement sensitivity and to be insensitive to external magnetic fields.

3.2.1. Rogowski Coil Current Sensor. The Rogowski Coil is a simple, inexpensive and accurate approach for current measurement. Structure of a Rogowski Coil is similar to a CT. However, instead of an iron core, Rogowski Coil is based on air or ironless bobbins with hundreds or thousand of turns, as shown in Figure 3.10. The Rogowski Coil has an air core, so it will never get saturated; therefore, its output of remains linear for high current measurement [101-106].
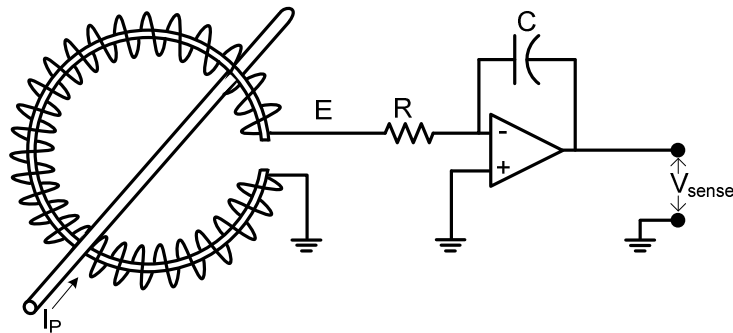
Figure 3.10. Rogowski Coil current sensor

The conductor from which the unknown current flows is surrounded by the Rogowski coil for current measurement, as shown in Figure 3.10. In order to place current carrying conductor inside, the Rogowski Coil can be opened without interrupting the circuit. The magnetic field produced by the current induces the voltage in the

secondary coil (E). Voltage E is proportional to the time derivative of current flowing through the conductor, which is given by (3.13).

$$E = M * \frac{dI_P}{dt} \tag{3.13}$$

Here, I_P is the unknown primary current and M is the mutual inductance of the circuit. M depends on the geometric parameters of the coil and is given by (3.14).

$$M = \frac{\mu_o A N_S}{l} \tag{3.14}$$

Where μ_o is the permeability of free space, A is the cross sectional area of the coil, N_S is the total number of secondary winding turns, and l is the mean path length of the coil. Because the derivative of the direct current is zero, the Rogowski Coil current sensor can not measure dc currents. It is used to measure ac or pulsed dc current only.

The phase delayed secondary voltage is integrated to produce an output voltage (V_{sense}) which is proportional to current I_P. If the Rogowski Coil is used to measure the current in a semiconductor switch, a simple resistor-capacitor integrator, as shown in Figure 3.10, can be used to reproduce current waveform as a voltage. Rogowski Coil terminals are connected in a special way to avoid the external field effects. The output voltage of the integrator circuit is given by (3.15), which is proportional to unknown current I_P.

$$V_{sense} = \frac{1}{RC} \int E * dt = \frac{1}{RC} \frac{\mu_0 A N_S}{l} I_P \tag{3.15}$$

This technique is also used when approximate current is not known before application. It measures high energy current pulses with high frequency harmonic content because upper bandwidth can extend into the mega-hertz range. A higher bandwidth (100 kHz) allows the Rogowski Coil to measure switching transients in semiconductors. Other advantages include a wide dynamic range (from milli-amps to thousands of amps), easy calibration, linear output, and accurate respond to transient currents, which makes it ideal for protecting systems and measuring current pulses. The Rogowski Coil sensor also has some disadvantages. Absolute value of the waveform cannot be reproduced using a Rogowski Coil. Also, voltage E is very small for hundreds of ampere current (rather than thousands) at typical power frequency, so it requires a high gain integrator. It is also difficult to satisfactorily connect a Rogowski Coil to the integrator to avoid ringing and reflections.

The Rogowski Coil works with a wound coil. The mechanically open structure of Rogowski Coil can create a slight gap in coil structure, which leads to errors (below 1% with a maximum of 2%) based on the position of the current carrying conductor in the aperture. This method's accuracy is affected by the external field due to the manufacturing tolerance of the wound coil. Planar Rogowski Coil current sensor is the solution to these problems.

3.2.2. Planar Rogowski Coil Current Sensor. A planar Rogowski Coil current sensor, used to measure ac or pulsed dc current, is an air core approach based on planar magnetic sensors, as shown in Figure 3.11[107-110]. It operates on the basic Rogowski coil principle in which a coil is magnetically coupled with the flux created by the current to be measured. In place of a continuous uniform coil used in the Rogowski Coil current

sensor, planar Rogowski Coil current sensor uses discrete coils placed at regular intervals on a fixed perimeter.
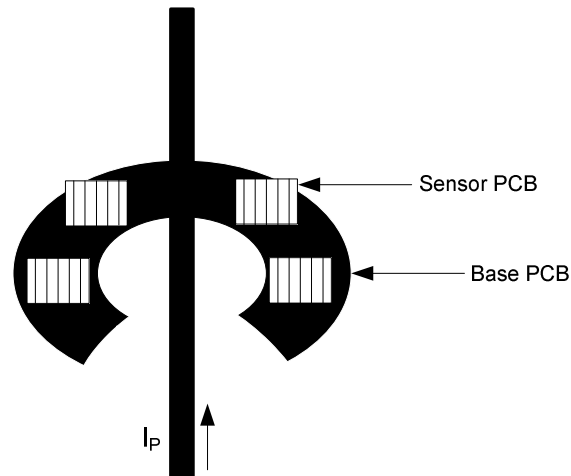
Figure 3.11. Planar Rogowski Coil current sensor

As shown in Figure 3.11, the planar Rogowski Coil current sensor consists of two parts; sensor PCB and base PCB. Each sensor PCB is made of two distinct air cored coils constructed on a multi layer PCB. Sensor PCBs, which are placed at right angle to the base PCB, are connected in a series to form inner and outer concentric loops, as shown in Figure 3.12. The great number of sensor PCBs gives lower sensitivity to conductor position, higher accuracy, and robustness to external field perturbations.

The current carrying conductor is placed inside the two loops without any electrical or mechanical interruption. Similar to a Rogowski Coil current sensor, the continuously changing magnetic flux due to current carrying conductor creates a voltage drop, which needs to be integrated. The integrator is kept very near to the current sensor

to reduce stray inductive pick up that can give rise to errors. The sense voltage V_{sense} in Figure 3.12 is given by (3.16).

$$V_{sense} = V_{inner} - \frac{V_{outer}}{\lambda} = V_{inner}\left(1 - \frac{V_{outer}}{V_{inner} * \lambda}\right)$$

(3.16)

Where V_{inner} and V_{outer} are voltages induced in the inner and outer loop, respectively.
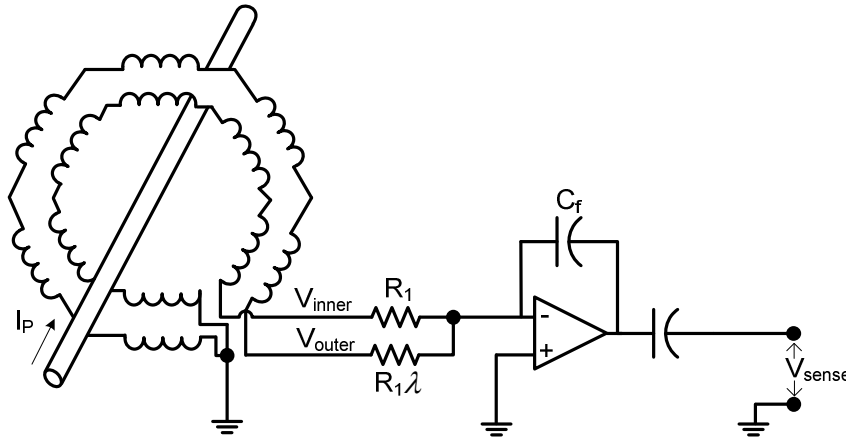
Figure 3.12. Planar Rogowski Coil current sensor with two concentric loops

In order to cancel the external field effect, this sensor is designed in such a way that ratio V_{outer}/V_{inner} is almost constant, irrespective of the position and magnitude of the external current source. Making $\lambda = (V_{outer}/V_{inner})$ force the voltage V_{sense} in (3.16) zero, in the other words, an external current source will not produce any signal at output. To measure current of current carrying conductor which is placed inside the loops, the sensor is designed such that $(\lambda/2) = (V_{outer}/V_{inner})$ irrespective of the position of current carrying

conductor. As a result, voltage V_{sense} in (3.16) is ($V_{inner}/2$); therefore, only half of the signal collected by inner loop is used for measurement.

This technique's advantages include its large bandwidth (10 Hz to 100 kHz), light weight, no magnetic saturation, low power consumption, low thermal losses, wide current measuring range, and high accuracy.

3.3. CURRENT MEASUREMENT TECHNIQUES USING HALL-EFFECT

Hall-effect sensors are used to measure ac, dc, and complex currents with electrical isolation. They are used to measure the current without interrupting the circuit. A Hall-effect sensor is small, provides noise-immune signal, and consumes little power [111-115]. A Hall-effect sensor works based on the Lorentz force, which acts on charges moving through a magnetic field. Figure 3.13 represents the Hall-effect principle. The Hall-effect principle states that when a magnetic field is applied to a conducting or semi conducting material from which current is flowing, a voltage will be developed across the sides of the material.
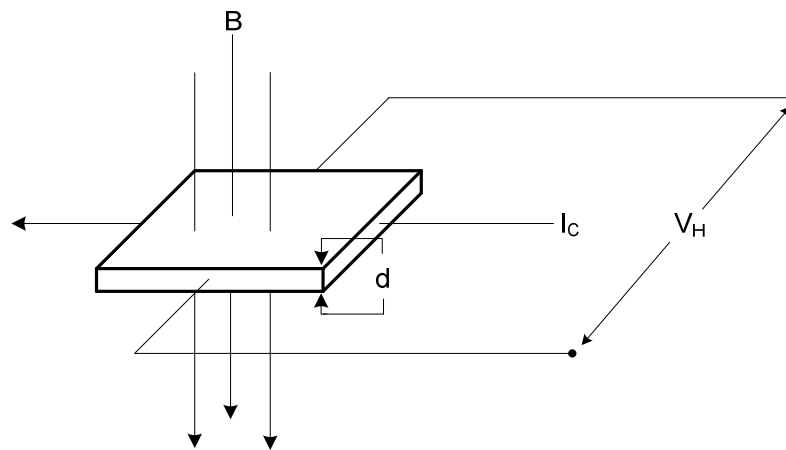
Figure 3.13. Hall-effect principle

If I_C is the control current passing through the Hall sensor, B is magnetic flux density created by unknown current carrying conductor, K is a constant of conducting material, d is the thickness of the sheet, and V_{OH} is the offset of the Hall sensor in the absence of the external field, the output Hall voltage V_H of Hall-effect sensor is given by (3.17).

$$V_H = \frac{K}{d} B I_C + V_{OH} \qquad (3.17)$$

Here, product $(K/d)*I_C$ represents the sensitivity of the Hall-effect sensor. However, the sensitivity and voltage V_{OH} of a Hall-effect sensor are temperature dependent. As per (3.17), if constant current I_C is supplied to the Hall-effect sensor, then a voltage is produced that is proportional to flux density B in the core, which is proportional to unknown primary current I_P. Hall-effect sensors are also known as Hall generators.

Flux density B for a Hall-effect sensor is inversely proportional to the distance from the center of the conductor to the point of sensing, so usable flux density cannot be achieved at much greater distance from the conductor's center. Other disadvantages of Hall-effect sensors are their low sensitivity, which requires a concentrator, tricky mechanical positioning, limited linearity range, sensitivity to mechanical stresses and ambient temperature variations, limited maximum frequency range due to junction capacitance, and requirement of an isolated power supply. Different Hall-effect-based current measurement techniques have been proposed to overcome the abovementioned disadvantages. These techniques include open-loop Hall-effect sensing, closed-loop Hall-effect sensing, and combinations of open-loop or closed-loop Hall-effect sensing with a current transformer technique.

3.3.1. Open-loop Hall-Effect Current Sensor. An open-loop Hall-effect current sensor uses a high permeability magnetic core (as a field concentrator) with an air gap located around the conductor which carries current I_P, as shown in Figure 3.14 [116-118].
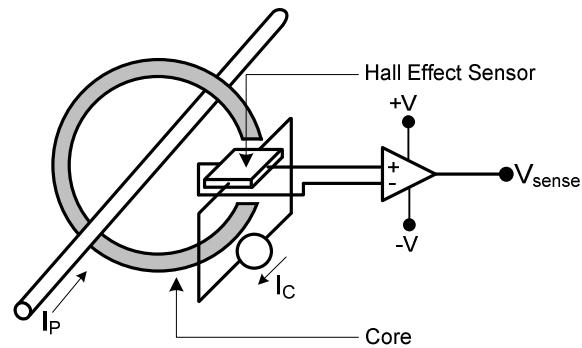
Figure 3.14. Open-loop Hall-effect current sensor with single turn primary

A linear Hall sensor is inserted into the air gap and provides voltage V_H proportional to flux density B produced by current I_P. Voltage V_H is amplified and output voltage is then read as a voltage which represents current I_P through a scaling factor. B-H loop for open-loop Hall-effect sensor is depicted in Figure 3.15. Voltage V_H is proportional to flux density B, and flux density B is proportional to current I_P within the linear region of hysteresis loop of the material used for the magnetic circuit, as shown in Figure 3.15. Voltage V_H needs to be amplified and compensated to remove the offset component.

Open-loop Hall-effect current sensors are able to measure ac, dc, and complex currents accurately. The benefits of an open-loop Hall-effect current sensor include

simple construction, low cost, low power consumption, low insertion losses, and small size for higher currents.
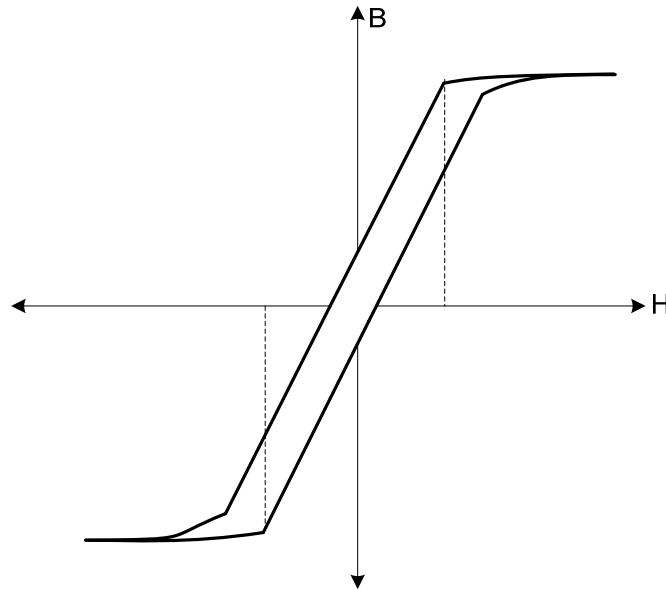
Figure 3.15. B-H loop for open-loop Hall-effect current sensor

However, disadvantages include magnetic core heating due to core losses at high frequency current measurement, narrow bandwidth (dc to 25 kHz), high offset and gain drift, limited range of linearity, and lower accuracy.

In order to get higher accuracy for lower current measurements (<50A), the multiple turns of the conductor from which unknown current is flowing is wrapped around the field concentrating core as shown in Figure 3.16 [119]. The problem with this sensor is that the coil wrapped around the gaped core creates an inductor. Furthermore, core losses are increased by the square of the primary ampere turns in this case.
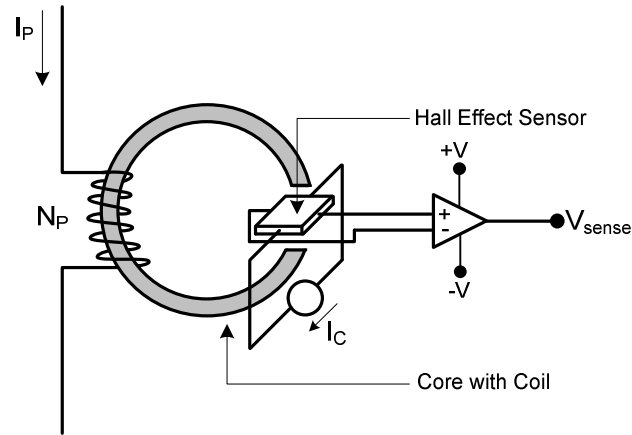
Figure 3.16. Open-loop Hall-effect current sensor with a multi-turn primary

3.3.2. Closed-loop Hall-Effect Current Sensor. Closed-loop Hall-effect current sensor improves the performance of open-loop Hall-effect current sensor by using a compensation circuit, as shown in Figure 3.17. In closed-loop Hall-effect sensor, a low current secondary winding is wrapped around the high permeability core to develop magnetic flux in opposition to the flux developed by current I_P [116]. The hall sensor is enclosed in an overall feedback loop, as depicted in Figure 3.17 [120-122]. A Hall sensor in the air gap produces a voltage V_H proportional to flux density in the core. Voltage V_H is then amplified by the operational amplifier and fed into a push-pull amplifier. Compensation current I_S is fed by the push-pull amplifier into the secondary coil to null the flux in the core.

The Hall sensor in the air gap is also used to detect zero flux. Therefore, the closed-loop Hall-effect sensors are also known as compensated or zero flux Hall-effect current sensors. Current I_S creates flux equal in amplitude, but opposite in direction, to the flux created by current I_P. Operating the core near zero flux eliminates dependence on the linearity of the core and Hall sensor and also reduces hysteresis errors.
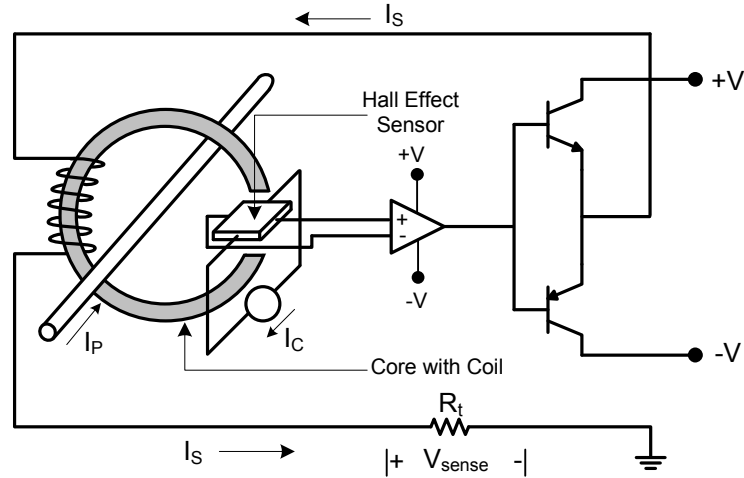
Figure 3.17. Closed-loop Hall-effect current sensor

When the magnetic flux is fully compensated, the ampere turns of two windings are identical, which is given by (3.18).

$$N_P I_P = N_S I_S \qquad (3.18)$$

Therefore, current I_S, according to (3.18), is exact representation of unknown current I_P. The frequency response of the closed-loop Hall-effect current sensor is enhanced due to the zero flux. Current I_S can be converted to a voltage by placing a resistor R_t from the output of the secondary coil to ground, as shown in Figure 3.17. By selecting the proper value of resistor R_t, the voltage can be scaled for any application. A capacitor can be added in parallel to resistor R_t to filter high frequency components in the feedback signal.

Closed-loop Hall-effect current sensors are able to accurately measure ac, dc, and complex currents. Closed-loop Hall-effect current sensors provide many advantages, such

as high bandwidth (dc to 200 kHz), high accuracy and linearity, fast response time, low insertion losses, and low gain drift. However, their disadvantages include higher cost, high current consumption, larger dimensions, and limited output current due to the fact that closed-loop sensors can only drive a finite amount of secondary current. It is very difficult to design closed-loop Hall-effect sensors that will operate from low secondary voltage power supplies (less than or equal to 5 V) with primary currents more than 25 A. In closed-loop Hall-effect sensor, there is very limited voltage to drive a proper secondary winding and terminating resistance. Solution to this problem is combination of an open-loop Hall-effect current sensor with a current transformer.

3.3.3. Combination of an Open-loop Hall-Effect Current Sensor with a Current Transformer. This sensor's construction is similar to closed-loop Hall-effect current sensor with same magnetic circuit, Hall sensor, and secondary winding, as depicted in Figure 3.18 [116].
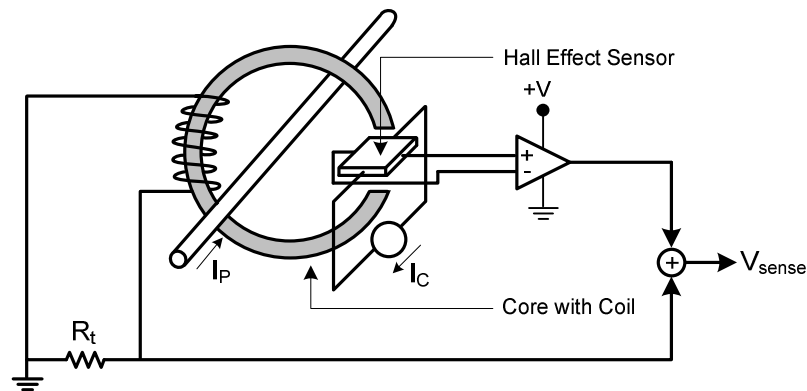
Figure 3.18. Combination of an open-loop Hall-effect current sensor and a current transformer

This technique combines the desirable properties of an open-loop Hall-effect current sensor and a CT [123-125]. It works as an open-loop Hall-effect sensor at low frequencies (2-10 kHz) with Hall generator providing signal proportional to current I_P. At high frequencies (10-100 kHz), this sensor works as a CT, where the output current is proportional to the ac current I_P. In this method, for flux measurement, a high performance application specific integrated circuit with temperature compensated Hall sensor is added in the gap of high permeability magnetic core, as depicted in Figure 3.18. It provides enhanced accuracy when this sensor is working as an open-loop Hall-effect sensor to measure dc and low frequency currents. Hall sensor and transformer signals are electronically added to form a common output signal. This sensor requires very low secondary power consumption because the power supply is not required to drive the secondary coil with compensation current I_S

This technique provides broad bandwidth, as shown in Figure 3.19, because the open-loop Hall-effect sensor adds the dc response to the high frequency capability of the current transformer.
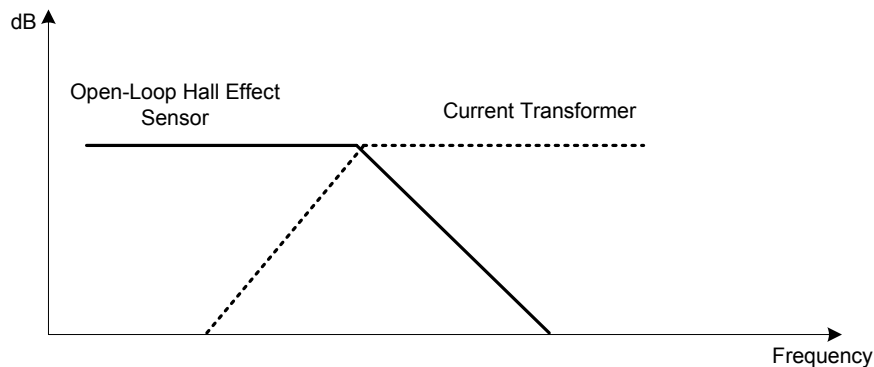
Figure 3.19. Broad bandwidth provided by combination of an open-loop Hall-effect current sensor and a current transformer

This technique is able to measure dc, ac, and complex currents with galvanic isolation and low insertion loss. Its construction is the same as that of a closed-loop Hall-effect current sensor; therefore, it does not provide any prize advantage. Other advantages include low power consumption, suitability for small secondary supply voltages, high bandwidth (dc to 100 kHz), and fast response time. Disadvantages include offset and gain drift, large core size at low frequency, need for a large secondary coil for high frequency detection, and moderate accuracy. It is also possible to combine a closed-loop Hall-effect current sensor with a CT. More information about this technique is given in [119].

3.4. SATURABLE INDUCTOR CURRENT SENSORS

Saturable inductor current sensors work on the same measurement principle as Hall-effect-based current sensors: the magnetic field created by the primary current to be measured is detected by a specific sensing element [116, 126]. The design of the saturable inductor current sensor is similar to that of a closed-loop Hall-effect current sensor; the only difference is that this method uses the saturable inductor instead of the Hall-effect sensor in the air gap, as shown in Figure 3.20.

Saturable inductor current sensor is based on the detection of an inductance change. The saturable inductor is made of small and thin magnetic core wound with a coil around it, as depicted in Figure 3.21. The saturable inductor operates into its saturation region. It is designed in such a way that the external and internal flux density will affect its saturation level. Change in the saturation level of a saturable inductor will alter core's permeability and, consequently, its inductance L. The value of saturable inductance (L) is high at low currents (based on the permeability of the core) and low at high currents (the core permeability becomes unity when saturated).
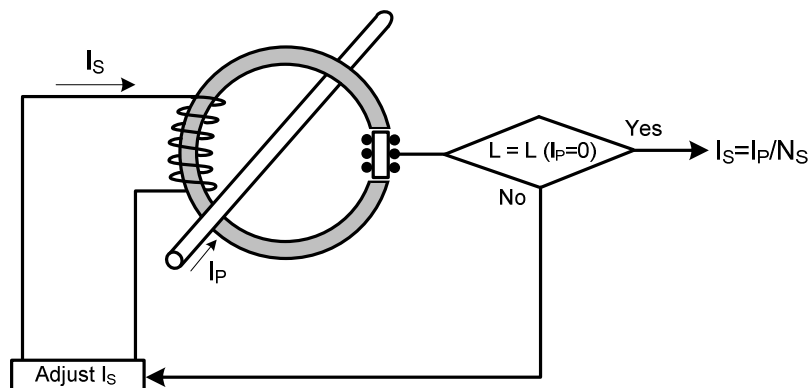
Figure 3.20. Saturable inductor current sensor

As shown in Figure 3.21, the saturable inductor current (I_{sic}) passes through the coil wrapped around inductor, which produces the flux density B_{sic} in addition to the flux density B_P produced by current I_P.
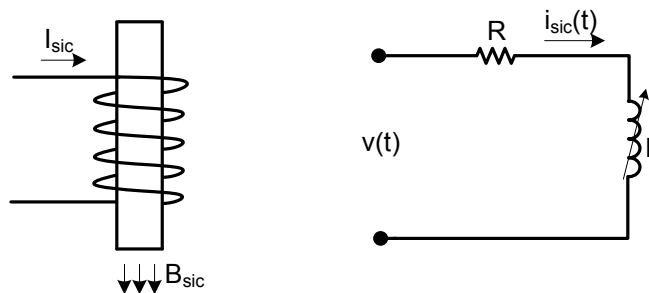
Figure 3.21. Saturable inductor and its equivalent circuit

When overall flux (due to I_P and I_{sic}) is high, the core gets saturated and L drops. At lower flux, the value of L is high. If polarity of current I_{sic} gets change, the direction of the flux created by it will also change. If fluxes created by currents I_P and I_{sic} are opposite and have the same magnitude, they will create zero total flux. Saturable inductor is

designed to provide high L at zero total flux. As shown in Figure 3.20, the variations of L are detected by sensor electronics and compensated by using compensation current I_S, such that the total gap field is zero.

The current response of a saturable inductor to a voltage a voltage step when flux density due to current I_P and I_S ($B_{P\&S}$) is zero and non-zero is illustrated in Figure 3.22.
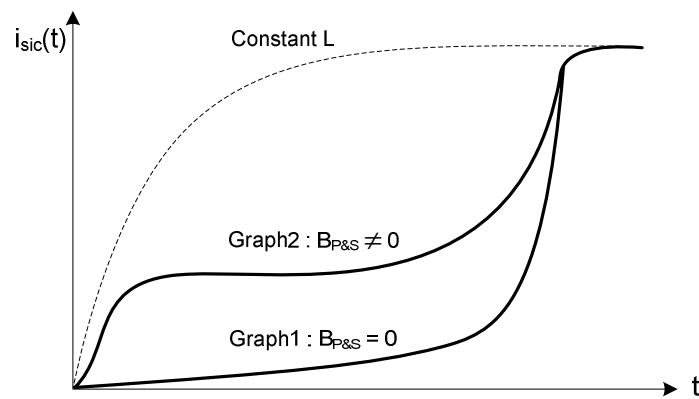
Figure 3.22. Current response of a saturable inductor to a voltage step

The graph for constant L shows the expected exponential current response. Graph-1 shows the current response of saturable inductor when $B_{P\&S}$ is zero. For a small value of current I_{sic}, the inductor is non-saturated. When current I_{sic} exceeds the pre-defined level, the value of L drops, which results in fast current change. Graph-2 shows the current response of the saturable inductor when $B_{P\&S}$ is non-zero. For small I_{sic} value, $B_{P\&S}$ is predominant so L drops. When flux densities B_{sic} (due to current I_{sic}) and $B_{P\&S}$ are equal and opposite, the value of L is high, resulting in low current variation. As current I_{sic} continues to grow, the field caused by it becomes predominant. This leads the core

into opposite saturation, so L drops. The asymptotic level of current is defined by excitation voltage v(t) and coil resistance R (see Figure 3.21).

The current response of a saturable inductor when the square wave voltage is given as a supply in Figure 3.21 and flux density $B_{P\&S}$ is zero and non-zero is illustrated in Figure 3.23.

(a)

(b)
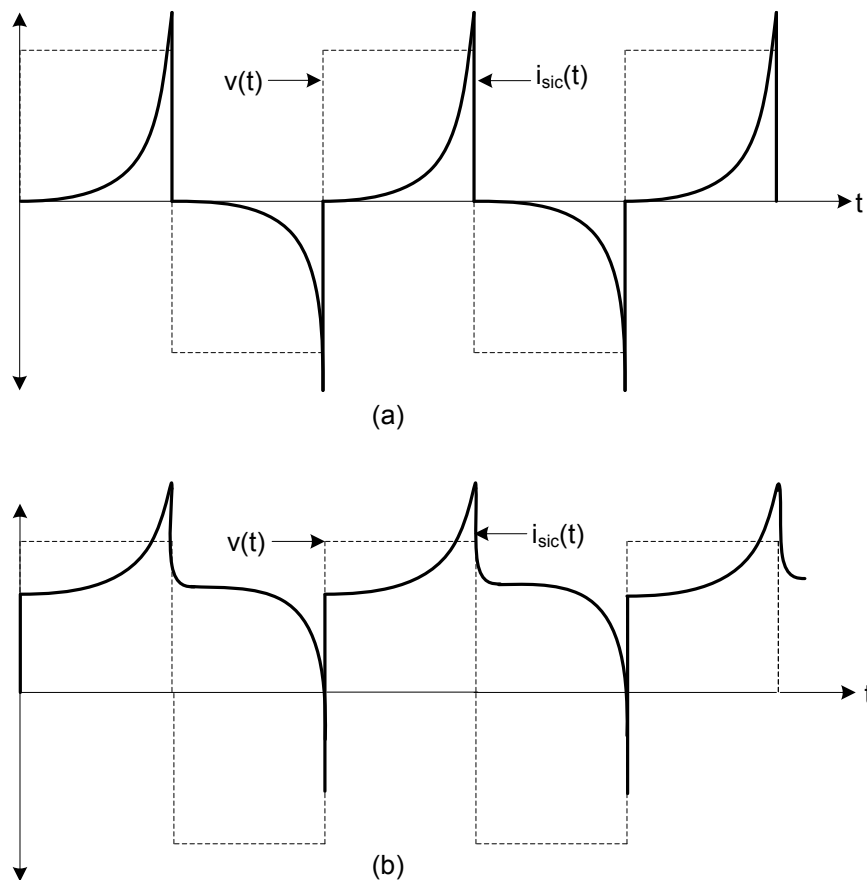
Figure 3.23. Voltage steps and current response of a saturable inductor; when (a) $B_{P\&S} = 0$, and (b) $B_{P\&S} \neq 0$

If no primary current I_P is applied (or $B_{P\&S}$ is zero), and the square wave voltage v(t) is given as a supply to saturable inductor in Figure 3.20, the behavior of current I_{sic} is

depicted in Figure 3.23(a). The shape of current I_{sic} is same as shown in Figure 3.22 for zero flux density $B_{P\&S}$. If the loop in Figure 3.20 is not closed and current I_S is not available, the behavior of current I_{sic}, when primary current I_P is present (or $B_{P\&S}$ is non-zero), is given in Figure 3.23(b). The differences in two waveforms are the peak amplitude and dc current component. Different techniques used to sense the value of L in Figure 3.20 are measuring the dc current component, measuring the amplitude of the second harmonic, or measuring the duty cycle of the voltage of the Figure 3.23(b). Once the changes in L are detected, the closed-loop in Figure 3.20 is used to compensate the flux in the gap.

In this technique, high frequency performance is achieved by using two cores without air gaps. One of the two main cores is used to create a saturable inductor and the other is used to create a high frequency transformer effect. In another approach, three cores can be used without air gap. Two of the three cores are used to create saturable inductor, and the third core is used to create a high frequency transformer effect. More information about these techniques is given in [110] and [126]. It is difficult to compare different saturable inductor techniques. Advantages of saturable inductor sensors include high resolution, high accuracy, low offset and gain drift, and large bandwidth (up to 500 kHz). Drawbacks of saturable inductor technologies include limited bandwidth for simpler design, relatively high secondary power consumption, and risk of current or voltage noise injection into the primary conductor.

3.5. MAGNETO-RESISTIVE CURRENT SENSOR

Every conducting material has some magneto-resistance. This magneto-resistance effect is large in pemalloys (Fe-Ni) and other ferromagnetic materials. A magneto-

resistor (MR) is a two terminal device which changes its resistance parabolically with applied magnetic field as shown in Figure 3.24. This variation of the resistance of MR due to the magnetic field is known as the anisotropic magneto-resistive (AMR) effect.
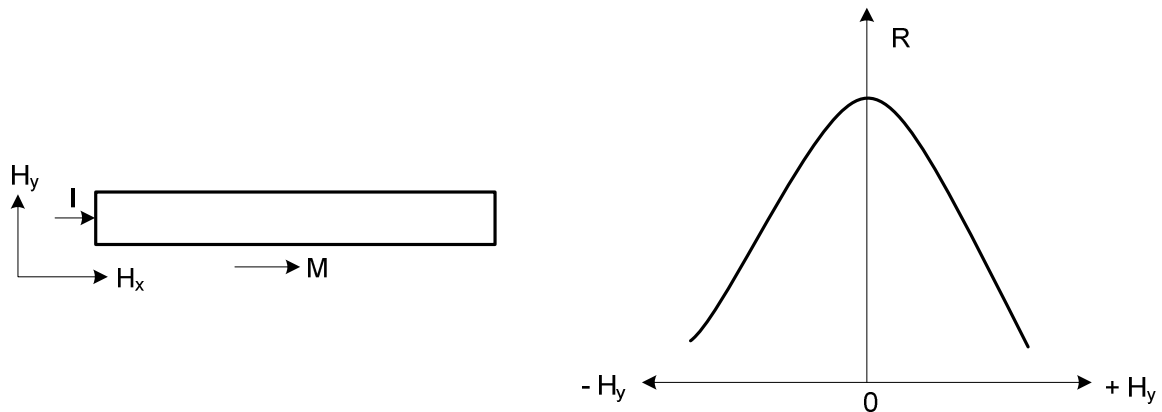
Figure 3.24. MR strip and resistance verses magnetic field for MR device

MR devices are more sensitive to magnetic field than are Hall-effect sensors. An MR device with a larger sensitivity is known as a giant magneto-resistor (GMR) [127]. An MR strip is depicted in Figure 3.24. Here H_y is the applied magnetic field, H_x is the internal or external (auxiliary) magnetic field, and M is the resultant magnetization due to H_y and H_x. Magnetic field H_y is coupled with an MR device and change the resistivity of the stripe, which is measured by the current I passing through the element. MR sensor sensitivity is controlled by controlling field H_x. When current I and magnetization M are parallel, the resistance of the strip is the greatest; when they are at a 90° angle to each other, it is the lowest [128-131].

An MR device cannot detect the direction of field H_y and has vanishing sensitivity for low fields. Other disadvantages include limited linear range, poor temperature characteristics, and a wide range of sensitivity from device to device. Non-linearity and non-directionality of an MR device are corrected by modifying the MR transfer curve, as shown in Figure 3.25.
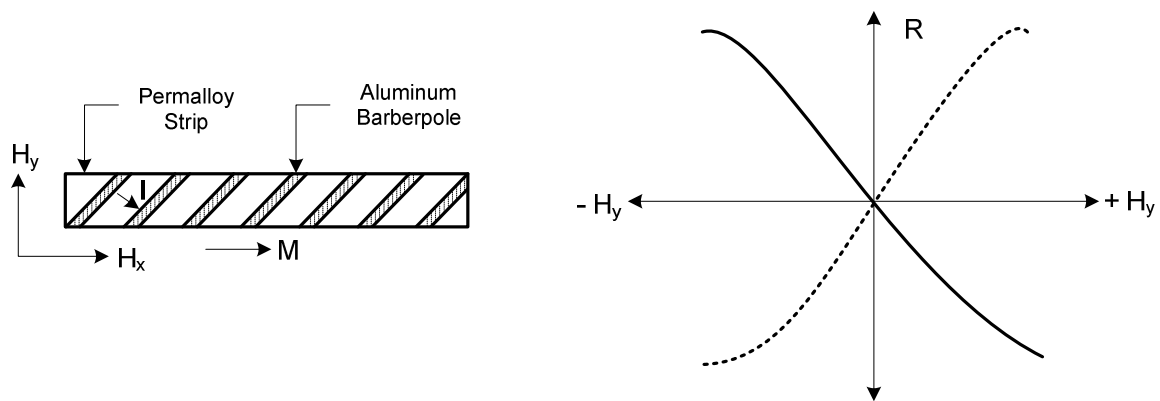
Figure 3.25. Barberpole MR device and resistance verses magnetic field for barberpole MR device

The most common way to modify the MR transfer curve is the use of barberpole configuration. Small structures of a highly conductive material such as aluminum are added to the MR stripe at an inclination of $|45°|$ to create the barberpole configurations. Barberpoles are tiny blocks of material sitting on top of the permalloy. One of such configuration with $+45°$ inclination of barberpoles is shown in Figure 3.25 ($-45°$ between current I and H_X-axis). Aluminum has a resistivity about five times lower than that of permalloy, so the barberpoles cause a change of operating point by changing the direction of current, as shown in Figure 3.25. With $45°$ barberpole biasing, if field H_Y increases,

the resistance of barberpole MR device decreases, and if field H_Y decreases, the resistance of barberpole MR device increases, as shown by a solid line in the graph of Figure 3.25. The dashed line in the graph of Figure 3.25 shows the inverse behavior of barberpole MR device with -45° barberpole biasing.

External magnetic fields can distort the current measurement of barberpole MR senor. To avoid this distortion, barberpole MR devices can be configured into a half bridge or a full bridge arrangement. In the Wheatstone bridge configuration, shown in Figure 3.26, the arms of the bridge are made of four highly symmetrical MR devices.
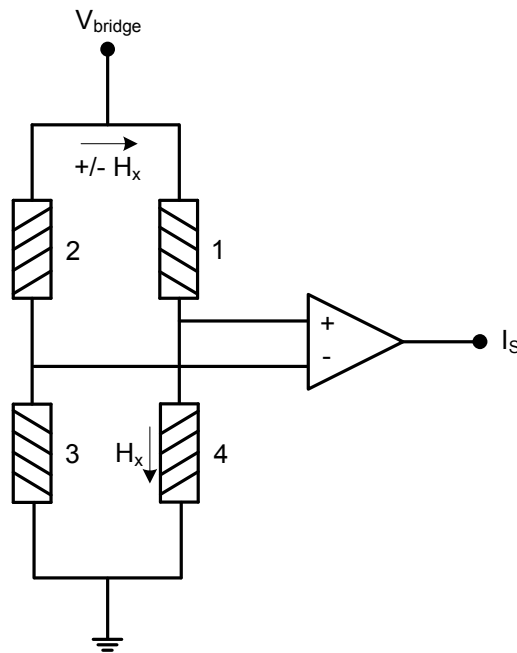
Figure 3.26. Four barberpole MR devices in a Wheatstone bridge configuration (1 and 3 with 45° and 2 and 4 with -45° barberpole biasing)

As shown in Figure 3.26, in one arm of the bridge, the barberpoles are placed in opposite directions above the two MRs, such that, in the presence of a magnetic field, the

value of the first resistor increases and the value of the second decreases. The individual barberpole MR devices still sensitive to the temperature change; however, they all change at the same rate yielding a zero net drift at the output of the bridge.

Even with the barberpoles, the linearity of MR device is not very high; therefore, a compensation circuit is required, as in the closed-loop Hall-effect current sensor. An electrically isolated aluminum compensation conductor is integrated on the same substrate above the permalloy resistors as shown in Figure 3.27.
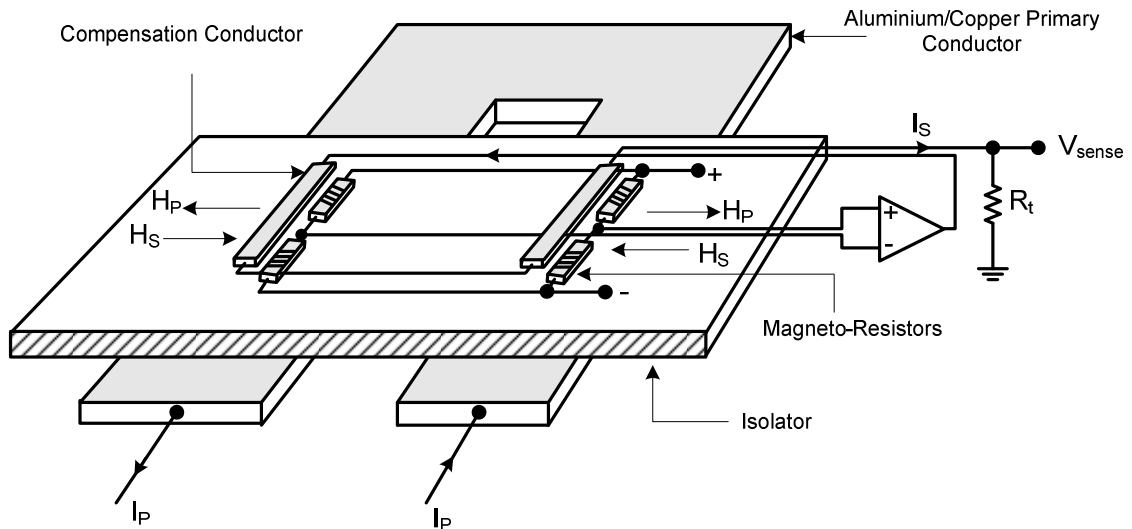
Figure 3.27. Barberpole MR sensors with compensation circuit

The output of the Wheatstone bridge is connected to the input of an operational amplifier, which generates the compensating current (I_S). Current I_S then flows through the aluminum conductor to generate a magnetic field that exactly compensates the field created by current I_P. The bridge output voltage is usually close to zero; therefore, sensor nonlinearity is minimized. Current I_S is then measured through resistor R_t, which is a

exact representation of the current I_P. In order to have the same amplitude but opposite directions of the magnetic fields on two arms of the bridge, the primary current conductor under the substrate is U-shaped. More information about this technique is given in [131].

An MR current sensor is able to measure dc and ac currents accurately with galvanic isolation. Advantages of this technique include small size, wide bandwidth (dc to 100 kHz), and no remenance during overload. However, precise positioning of the barberpole MR device in the Wheatstone bridge is required with respect to the current carrying conductor. Barberpole MR devices have to be matched one another in sensitivity and temperature drifts, so they need to be placed close together to eliminate the effect of temperature gradient.

3.6. FIBER OPTIC CURRENT SENSOR

A fiber optics current sensor (FOCS) determines the current flow in an electrical conductor by measuring the magnetic field density within the vicinity of the conductor [132-136]. The operation principal is based on the Faraday Effect. When a polarized monochromatic light propagates parallel to a magnetic field, the polarization direction rotates, as shown in Figure 3.28.

The polarization angle is proportional to the magnetic field circulation on the optical path. The angular rotation experienced by the light passing through the sensor is given by (3.19).

$$\theta = VBl \hspace{4cm} (3.19)$$

Where V is the Verdet constant of the material used for sensor, B is magnetic flux density, and l is the length of FOCS exposed to the magnetic field. The polarization angle

also depends on the light wavelength and fiber material. FOCS measures the exact integral of the magnetic field along the closed-loop created by the fiber. A true current reading is obtained if FOCS completely encloses the conductor; otherwise the reading reflects the magnetic field intensity at the measurement point and has to be scaled accordingly.
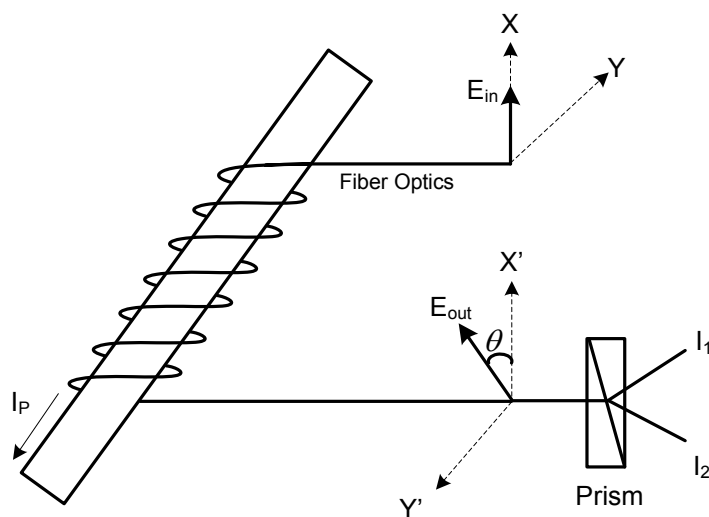
Figure 3.28. Polarimetric fiber optic current sensor

FOCSs are classified as intrinsic and extrinsic type. An intrinsic sensor uses fiber for current sensing, whereas an extrinsic sensor uses bulk optic. On the other hand, there are three different approaches of FOCS bulk, polarimetric, and interferometric. Bulk current sensor has high Verdet constant crystals, resulting in excellent sensitivity. Optical fiber has a lower Verdet constant, but many turns of the fiber around the conductor results in an improved sensitivity. The polarimetric sensor measures the rotation of a

linear polarization, while the interferometric sensor using a Sagnac interferometer measures the non-reciprocal phase shift.

FOCS offers many advantages over to conventional approaches. They can be used without any risk of discharge with the ground. Additionally, they offer a total protection against stray magnetic fields and have wide bandwidth that allows harmonic analysis of the measuring currents. They are very small; therefore, design of light and compact sensors is easy. Fiber optic sensor's installation is fast, simple, and can be done without interrupting the electric circuit to be measured. The built-in insulation of the optical fiber is an important characteristic for high voltage installations.

3.7. COMPARISION BETWEEN ELECTROMAGNETIC-BASED CURRENT SENSING TECHNIQUES

Table 3.1 summarizes the advantages and disadvantages of the presented electromagnetic-based current sensing techniques.

Table 3.1. Comparative overview of electromagnetic-based current sensing techniques

Techniques	Advantages	Disadvantages	Cost	Bandwidth	Measuring range
Using ACCT	Lossless, good SNR, good common mode rejection	Measures only ac current, core limitations, limited frequency range, not suitable for multiple-inductor converters	$3 (10A)	0.1Hz-100MHz	mA-kA
Using ACCT with sample-and-hold	Accurate, low power loss, able to measure ac current having dc current component	Requirement of high bandwidth sample-and-hold ICs and two transformers, core limitations	-	-	-

Table 3.1. Comparative overview of electromagnetic-based current sensing techniques (Cont.)

Techniques	Advantages	Disadvantages	Cost	Bandwidth	Measuring range
Using UCT	Lossless, accurately measures ac current having dc current component	Not suitable for higher switching frequencies, core limitations	-	-	-
Using DCCT	DCCT can work with primary currents in either direction	Limited bandwidth (<100 kHz), significant output distortion, need of accurate transformers, core limitations	-	-	50-2000A
Using Rogowski Coil	Accurate, low weight, no dc current saturation, low sensitivity to parameter variations, ac and pulsed dc current measurements	External circuit is required to analyze output, open structure leads to measurement error, error is introduced by processing electronics	-	10Hz–100kHz	0-10kA
Using planar Rogowski Coil	Lossless, ac and pulsed dc current measurements accurate, light and small, insensitive to external field perturbations and conductor position inside the coil	Expensive, external circuit is required to analyze output, complicated circuit, high secondary power consumption	$122 (400A)	10Hz–100kHz	0-10kA
Using open-loop Hall-effect current sensor	Low secondary power consumption, small size, low cost, ac, dc, and complex current measurements	Low sensitivity, temperature dependent output, linearity errors, porn to static drift, core limitations	$43 (300A)	0-25kHz	0-15kA
Using closed-loop Hall-effect current sensor	Accurate, ac, dc, and complex current measurements, fast response time, wide bandwidth, low temperature drift	Compensation circuit is required, high secondary current consumption, expensive, bulky for low currents, core limitations	$94 (300A)	0-200kHz	0-15kA

Table 3.1. Comparative overview of electromagnetic-based current sensing techniques (Cont.)

Techniques	Advantages	Disadvantages	Cost	Bandwidth	Measuring range
Using an open-loop Hall-effect current sensor with a CT	Unipolar supply, low power consumption, ac and dc, and complex current measurement, wide bandwidth	Linearity errors, low frequencies; offset and gain drift with temperature, moderate accuracy, core limitations	$21 (100A)	0-100kHz	25-150A
Using saturable inductor current sensor with one core	High resolution, high accuracy, ac and dc current measurement	Limited bandwidth, high secondary power consumption, core limitations	-	0-200kHz	0-500A
Using saturable inductor current sensor with two cores	Good resolution, accurate, wide bandwidth, good immunity to surrounding magnetic fields, ac and dc current measurement	Risk of current or voltage noise injection into the primary conductor, high secondary power consumption, core limitations	$636 (50A)	0-500kHz	0-150A
Using saturable inductor current sensor with three cores	High resolution, high accuracy, wide bandwidth, low noise on output signal, ac and dc current measurement	Limited operating temperature (10°-50° C), high secondary power consumption, large dimensions, costly, core limitations	$992 (300A)	0-100kHz	0-700A
Using MR current sensor	Smaller volume and weight, no remanence, ac and dc current measurement, high sensitivity, noise immunity	Placement of barberpoles in Wheatstone bridge configuration, limited frequency response due to magnetic inertia of permalloy and skin effect of current carrying conductor	$250 (<2A)	0-100kHz	0-50A
Using FOCS	Lossless, no electromagnetic interference, small sensing elements, ac and dc current measurement	Expensive, environmental sensitivity	-	10Hz-6kHz	up to 500kA

4. CURRENT SENISNG TECHNIQUES WITH SELF-TUNING AND/OR AUTO-CALIBRATION

In most measurement techniques, the accuracy of the measurement depends on some assumed parameter e.g. resistor value in resistive-based approaches. This assumed value is subject to temperature variations and inaccuracies. Due to these non-ideal effects, conventional current measurement approaches are sensitive to temperature, tolerance of components, noise, and operating conditions. The solution is self-tuning approaches in which the assumption that is made on the value of a parameter will tune itself [39].

4.1. MOSFET R_{DS}-BASED CURRENT SENSING TECHNIQUE WITH REAL-TIME SELF CALIBRATION

For accurate current measurement, it is necessary that circuit should somehow measure one of the current carrying elements in its path and sense the voltage across the same for accurate current measurement. One approach combines externally added sense resistor-based current sensing technique with another lossless method, such as MOSFET R_{DS}-based current sensing, filter-based current sensing, or observer current sensing for accurate current measurement. In Figure 4.1, externally added sense resistor-based current sensing method is combined with the MOSFET R_{DS}-based current sensing to effectively measure current I_L by determining the accurate value of resistance R_{DS}. Accuracy, along with losslessness, is achieved using an extra circuit which is a series connection of switch S_3 and resistor R_{sense} [137-139]. This extra circuit is added into the circuit infrequently for calibration purpose; therefore, the current rating of switch S_3 is small.
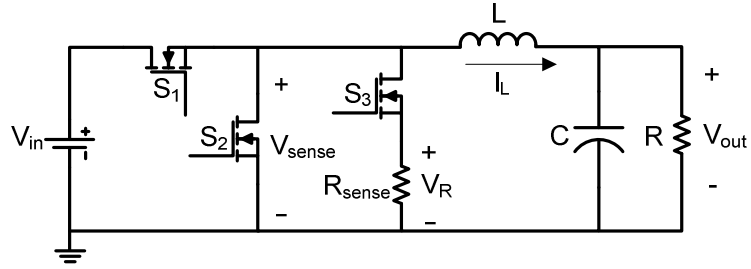
Figure 4.1. MOSFET R_{DS}-based current sensing technique with self-calibration

During a normal cycle, switch S_2 is on for interval $0<t<(1-d)T$ and current I_L is specified by (4.1).

$$I_L = \frac{-V_{sense}}{R_{DS}}$$ (4.1)

Resistance R_{DS} is initially estimated from the MOSFET datasheet. To find calibrated value of resistance R_{DS} (R_{DS_cali}), main switch S_2 is kept off, switch S_3 is turned on, and the voltage across resistor R_{sense} (V_R) is measured to find the value of current I_L, which is specified by (4.2).

$$I_L = \frac{-V_R}{R_{sense}}$$ (4.2)

If current I_L is not affected by the switching of S_3, from (4.1) and (4.2), the value of R_{DS_cali} is derived as (4.3).

$$R_{DS\_calib} = \frac{R_{sense}V_{Sense}}{V_R}$$ (4.3)

The accuracy of (4.3) depends on the value of the R_{sense}. The combined resistance of switch S_3 and resistor R_{sense} must be low enough, that the body diode of switch S_2 is not tuned on when switch S_3 is conducting. Another concern when finding the value of R_{DS_cali} is that the calibration cycle is performed only when the circuit is operating in steady state. If these conditions are satisfied, then the value of (4.3) is used in place of resistance R_{DS} in (4.1) to accurately find current I_L.

The slope of current I_L will increase if the combined voltage of switch S_3 and resistor R_{sense} is more than the voltage across switch S_2 (V_{sense}), introducing an error in current I_L (I_{L_error}), as depicted in Figure 4.2.
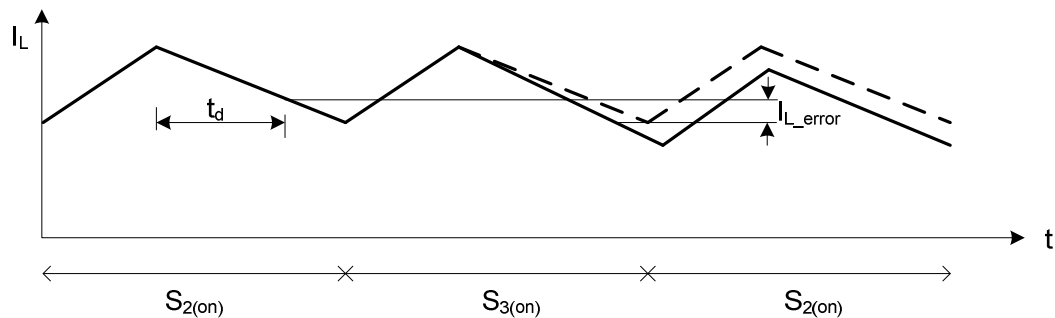
Figure 4.2. Error in the inductor current

In this situation, the value of error I_{L_error} must be found in order to find the correct value of R_{DS_calib}. However, this error can be large in converters having low output voltage and low inductance. I_{L_error} can be measured if the values of inductor L and the time delay t_d for sampling are known. The error I_{L_error} is calculated by using (4.4).

$$I_{L\_error} = t_d \left(\frac{V_{sense\_S_2(on)} - V_{sense\_S_3(on)}}{L} \right) \tag{4.4}$$

Once the value of I_{L_error} is known, the value of R_{DS_calib} is calculated using (4.5).

$$R_{DS\_calib} = R \frac{V_{sense\_S_2(on)}}{V_R} * \frac{1}{1 + \dfrac{I_{L\_error} R}{-V_R}} \tag{4.5}$$

The main difficulties with this method are the dependence on L and the need to find the values of voltages V_{sense} and V_R simultaneously. Once all of the above information is collected, then the value of (4.5) is used in (4.1) in place of R_{DS}, to find current I_L.

The error I_{L_error} is canceled by adjusting the duty cycle. There are three steps to achieve accurate current I_L measurement, as depicted in Figure 4.3.

1. When switch S_3 is on and switch S_2 is off, voltage $V_{sense\_S3(on)}$ is sensed to find the slope of the inductor current.

2. When switch S_2 is on and switch S_3 is off, duty cycle d is increased by Δd for compensation. The value of Δd, which does not depend on the value of L, is calculated by using (4.6).

$$\Delta d = \frac{V_{sense\_S_2(on)} - V_{sense\_S_3(on)}}{V_{in}} \left(\frac{t_d}{T_S} + (1-d) \right) \tag{4.6}$$

This increased duty cycle compensates the error in inductor current.

3. When switch S_3 is on and switch S_2 is off, voltage V_R is measured and used in (4.3) to find the value of R_{DS_calib}.
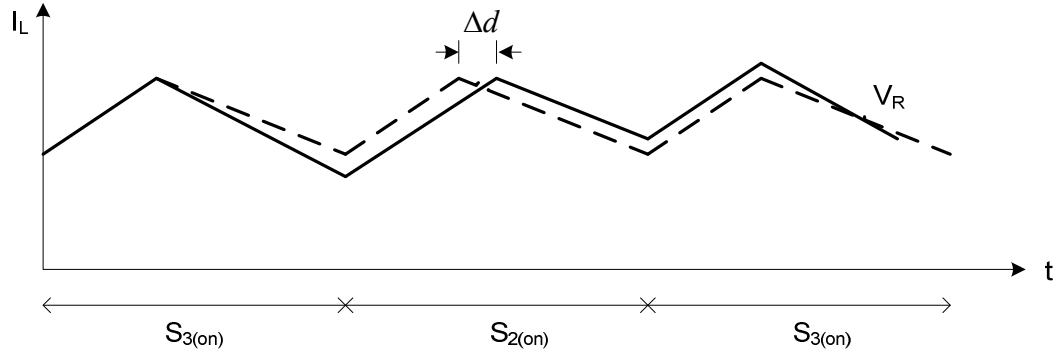
Figure 4.3. Duty cycle adjustment

4.2. CURRENT SENSING TECHNIQUE USING THE INTERNAL RESISTANCE OF AN INDUCTOR AND THE FILTER

The basic idea for this technique is taken from the resistive-based current sensing using external sense resistor method of Section 2. At higher frequencies, the parasitic equivalent inductance of resistor R_{sense} appears. Hence, it is necessary to compensate for the parasitic inductance. The equivalent circuit of R_{sense} for this case is given in Figure 4.4.
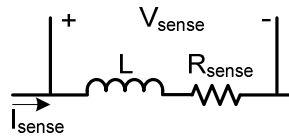
Figure 4.4. Equivalent circuit of R_{sense}

Voltage V_{sense} is given by (4.7).

$$V_{sense}(s) = (R_{sense} + Ls)I_{sense}(s) = K * I_{sense}(s) \tag{4.7}$$

At lower frequencies, voltage V_{sense} is proportional to current I_{sense}. At higher frequencies, gain K increases due to the parasitic inductance. A proper low pass filter, which can be active or passive, is required for compensating the gain K. Information about the use of an active filter for gain compensation is given in [140]. If a passive R_fC_f low pass filter is used, the voltage across the filter (V_{Cf}) is then given by (4.8).

$$V_{Cf}(s) = \left(\frac{R_{sense} + Ls}{1 + R_f C_f s} \right) I_{sense}(s) \tag{4.8}$$

As mentioned in Section 2, inductor windings have DCR or internal resistance R_L. It is possible to use the DCR of inductor L as R_{sense} and inductor L itself as parasitic inductor in above case. Therefore, the filter-based current sensing technique uses the resistor R_L of inductor L and passive filter R_fC_f, as shown in Figure 4.5, for accurate current sensing. The total impedance of the R_fC_f filter is same as the total impedance of L and R_L. This technique is currently popular because of its accuracy, losslessness, and high bandwidth [141, 142]. Other advantages of this technique include; continuous current measurement, low cost, PCB space saving, and power efficiency improvement.
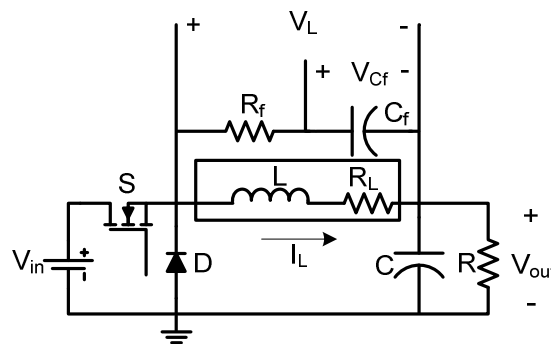
Figure 4.5. Filter-based current sensing technique

This technique detects the current I_L signal by sensing capacitor C_f voltage (V_{Cf}). Voltage V_{Cf} is given by (4.9).

$$V_{Cf}(s) = I_L(s) \left(\frac{R_L + Ls}{1 + R_f C_f s} \right)$$

(4.9)

The parallel $R_f C_f$ filter is designed in such a way that (4.10) and (4.11) are satisfied.

$$R_f C_f = \frac{L}{R_L}$$

(4.10)

$$\frac{L}{R_L} \gg T$$

(4.11)

Where $\tau_L = L/R_L$ is an inductor time constant and $\tau_C = R_f C_f$ is a low pass filter time constant. It is very difficult to satisfy (4.10). However, it is easy to satisfy (4.11) because the switching frequency is usually in the order of a few hundred kHz and resistance R_L is in mili-ohms.

If (4.10) and (4.11) are satisfied, the inductor current I_L is given by (4.12).

$$I_L = \frac{V_{Cf}}{R_L}$$

(4.12)

Figure 4.6 shows the response of voltage V_{Cf} and V_{RL} when time constants τ_L and τ_C match.
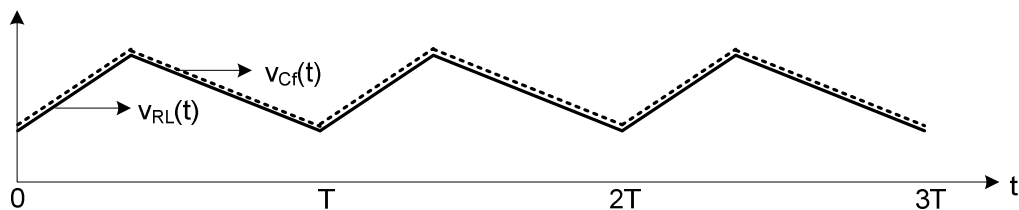
Figure 4.6. Voltage V_{Cf} and V_{RL}, when $\tau_C = \tau_L$

It is possible that the time constants will not match; one time constant can be greater or less than the other due to the tolerance of components, temperature dependence of R_L, and change in inductance due to dc current bias. Figure 4.7 shows the response of voltage V_{Cf} in steady state. When switch S is on, current I_L increases at a rate of $(V_{in}-V_{out})/(L)$ and capacitor C_f gets charged. When the freewheeling diode is on and switch S is off current I_L decreases at a rate of $(-V_{out})/L$, and capacitor C_f gets discharged. From charging and discharging rates, it is possible to find the slope of voltage V_{Cf}.
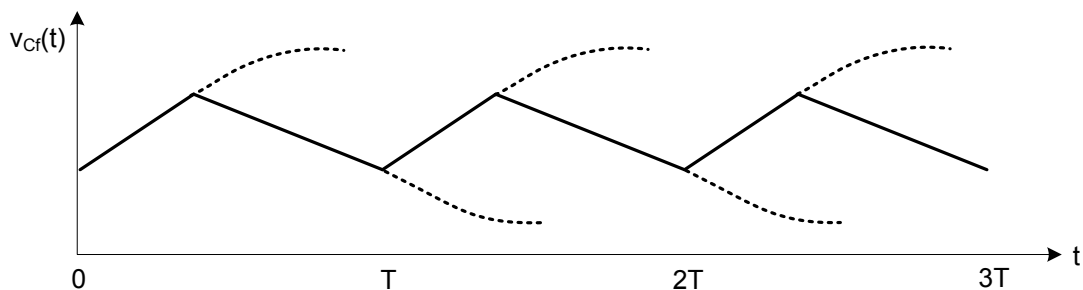
Figure 4.7. Voltage V_{Cf} in steady state

If time constants τ_L and τ_C are not matched, then peak to peak ripple of voltage V_{Cf} gets bigger or smaller than the peak-to-peak voltage ripple across resistor R_L

generated by ac component of the current I_L. This will change the slew rate of voltage V_{Cf} of Figure 4.7.

4.2.1. Filter-based Current Sensing with Temperature Compensation. An error is introduced in filter-based current sensing due to the temperature dependency of resistor R_L. To minimize this error, resistor (R_{Cf}) is added across the capacitor C_f for temperature compensation, as shown in Figure 4.8. R_{Cf} is the combination of resistors R_e, R_g, and R_{NTC}. R_{NTC} is a negative temperature co-efficient resistor. Information about the values of R_e, R_g, and R_{NTC} is given in [143]. Resistor R_{Cf} can also use for scaling down the detected current.
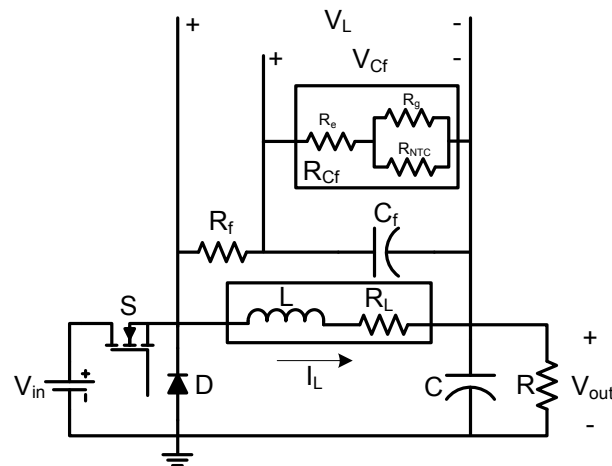
Figure 4.8. Filter-based current sensing with temperature compensated network

The addition of resistor R_{Cf} to the circuit changes the filter time constant. The new filter time constant is given by (4.13).

$$\tau_C = C_f \left(\frac{R_f R_{Cf}}{\left(R_f + R_{Cf} \right)} \right) \qquad (4.13)$$

If R_{Cf} is added to the circuit and time constants τ_L and τ_C are matched, the voltage V_{Cf} is given by (4.14). Figure 4.9 shows the illustration of voltage V_{Cf} and V_{RL} The dc voltage on the filter capacitor is level shifted by the factor $R_{Cf} / (R_{Cf}+R_f)$ in the presence of resistor R_{Cf}, as shown in Figure 4.9.

$$V_{Cf} = I_L \left(\frac{R_L R_{Cf}}{\left(R_f + R_{Cf} \right)} \right) \qquad (4.14)$$
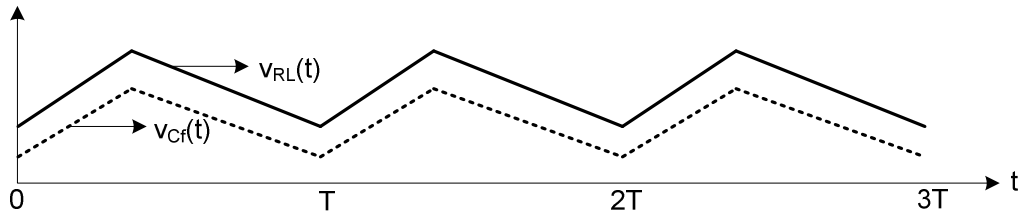
Figure 4.9. Voltage V_{Cf} and V_{RL}, when $\tau_C = \tau_L$, and resistor R_{Cf} is added into the circuit

4.2.2. Filter-based Current Sensing with Accurate R_L. If the filter-based current sensing technique depicted in Figure 4.5 is used for over current protection, and time constant τ_L is greater than time constant τ_C, the over current protection circuit can trip at a lower than desirable current. When time constant τ_L is less than time constant τ_C, the response is opposite. This is due to the fact that the value of R_L is not accurate; it is greater than the desired value. In order to deal with R_L parameter uncertainty, a modified

current sensing circuit for over current protection is shown in Figure 4.10 [145]. Design

steps for this technique are given below.
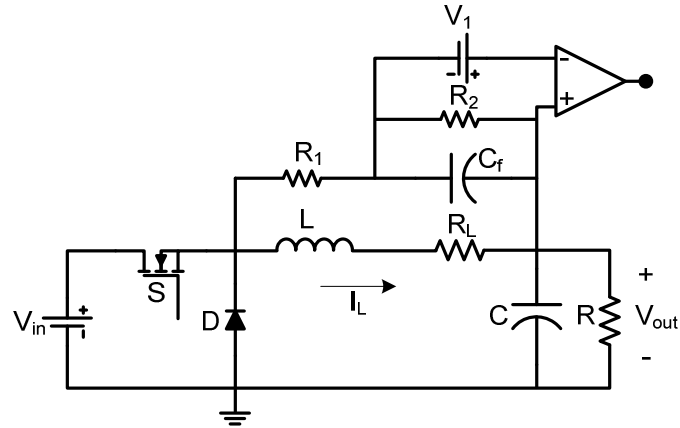
Figure 4.10. Filter-based current sensing with accurate R_L

If V_1 is the tripping voltage, I_1 is the tripping current, current I_1 is given by (4.15).

$$I_1 = \frac{V_1}{R_L} \tag{4.15}$$

In order to get actual value of R_L, a desired sense resistance R_{sense} can be

calculated from (4.16).

$$R_{sense} = \frac{V_1}{I_1} \tag{4.16}$$

Once the value of R_{sense} is known, then the value of inductor L can be found from

the value of R_L, which can be determined by (4.17).

$$R_L \geq R_{sense} \tag{4.17}$$

The maximum value of L at zero current and the minimum value of R_L at room temperature are measured to find value of time constant τ_C, as depicted in (4.18).

$$R_{f\,min} C_{f\,min} \rangle \frac{L_{max}}{R_{L\,min}} \tag{4.18}$$

If R_L is greater than R_{sense}, then the values of resistances R_1 and R_2 must be selected in such a way that (4.19) is satisfied.

$$\frac{R_2}{(R_1 + R_2)} = \frac{R_{sense}}{R_L} \tag{4.19}$$

R_f of Figure 4.5 is equivalent to the resultant resistance of the parallel connection between resistors R_1 and R_2 in Figure 4.10. R_L of Figure 4.5 is equivalent to $R_L*R_2/(R_1+R_2)$ in Figure 4.10.

4.2.3. Filter-based Current Sensing with Self-tuning. To overcome the time constants mismatching issue, a modified digital auto-tuning approach is presented in [146]. This technique automatically matches the time constants based on the measurement of the slope of voltage V_{Cf}, as depicted in Figure 4.11. The filter resistor R_f is variable.

A mismatch of time constants causes load transients, which create a large change in the value of voltage V_{Cf}. This change is sensed by a load transient detector. The controller measures the derivative of V_{Cf} signal and adjusts the value of variable resistor R_f to compensate for the time constant mismatch.
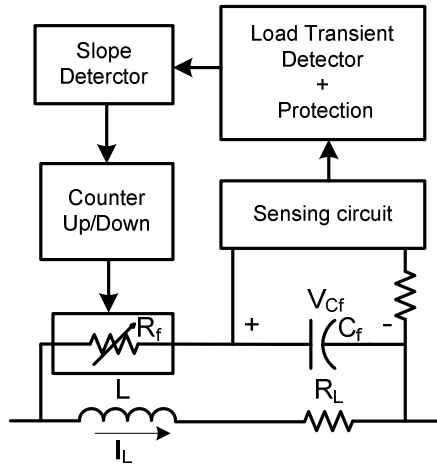
Figure 4.11. Digital auto-tuning circuit

4.2.4. Combined-Sense Technique. The sensed current in the filter-based current sensing has low magnitude and is susceptible to the interruption of noise, which is not acceptable in case of current-mode control [147]. In order to solve this problem, a new technique is introduced in [148] and shown in Figure 4.12. This technique provides better SNR of the sensed current.

Combined-sense technique includes additional switches S_3, S_4, resistor R_d, and capacitor C_d in filter-based current sensing, as depicted in Figure 4.12.
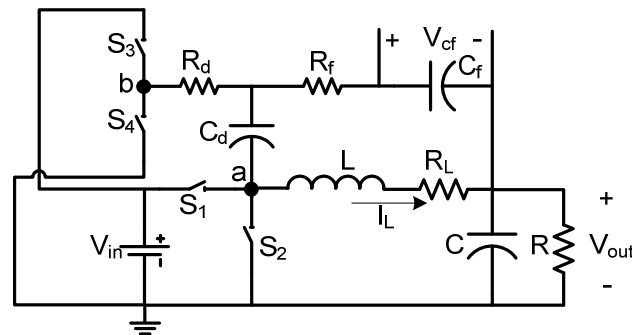
Figure 4.12. Combined-sense technique

Switches S_3 and S_4 are connected to node b. One end of their series connection is connected to V_{in} and the other is connected to the ground. Switches S_1 and S_2 are connected to node a. R_{DS} of switches S_1-S_4 are added into the filter according to the switching pattern. When switches S_1 and S_3 are on and S_2 and S_4 are off, the resistance of filter includes the R_{DS} of both switches S_1 and S_3. Similarly, when switches S_2 and S_4 are on and S_1 and S_3 are off, the resistance of filter includes the R_{DS} of both switches S_2 and S_4. In this way, the current can be sensed at any time during the cycle. The increased sense circuit resistance increases the voltage V_{Cf}, so the output signal is clean and less susceptible to noise. When the switches change their states from on to off or off to on, they temporarily fall into off state. The resistor R_d and capacitor C_d work as a low pass filter (R_dC_d) during this dead time to block the high frequency transient signal from affecting the current sense signal. The R_dC_d filter is also synchronize the operation of nodes a and b.

Voltages at points a and b (V_a and V_b) are depicted in Figure 4.13. Voltage V_a is a bit lower than voltage V_{in} and voltage V_b is approximately same as voltage V_{in}. because the rating of switches S_1 and S_2 are higher than the ratings of switches S_3 and S_4. Filter R_dC_d averages the voltage difference for cleaner and exact current measurement.
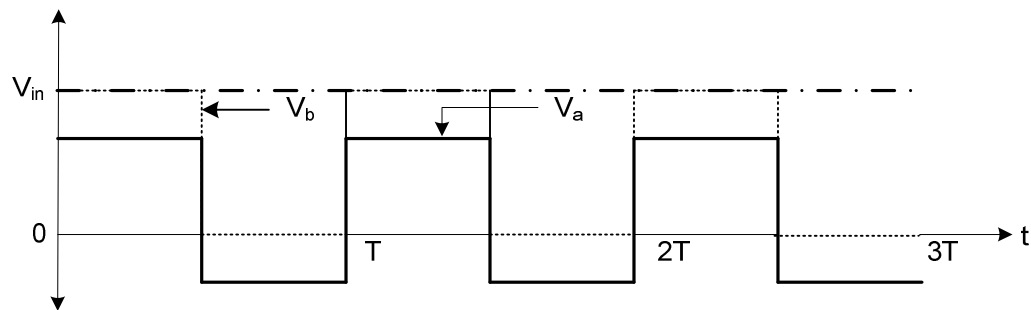
Figure 4.13. Voltages V_a and V_b in combined-sense technique

4.2.5. Filter-based Current Sensing with Self-tuning and Self-calibration. To achieve continuous current measurement with accuracy, losslessness, low switching noise, and high bandwidth, a modified technique is introduced in [149, 150] (see Figure 4.14).
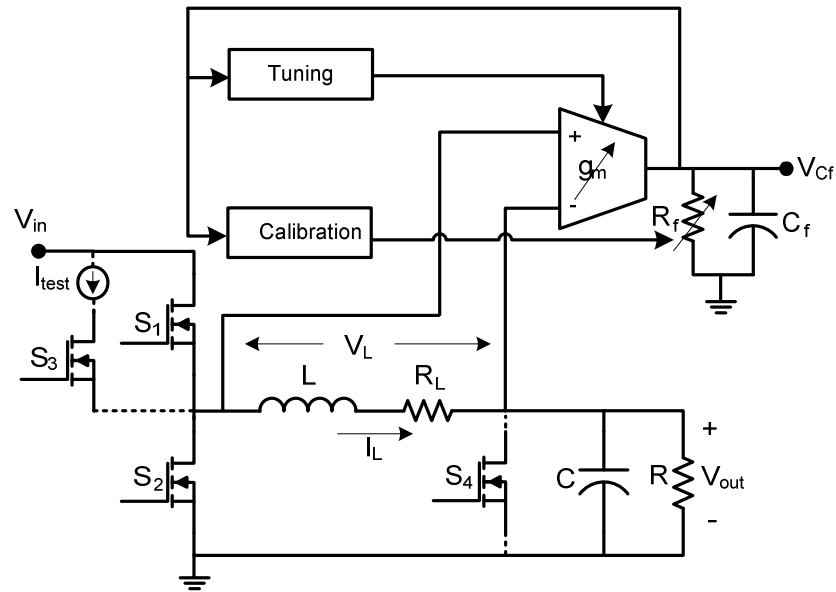
Figure 4.14. Filter-based technique with self-tuning and self-calibration

The sensed circuit is calibrated and tuned during the start-up and the inductor current is measured during normal operation, which ensures accuracy along with continuous current measurement benefits. The g_m-C_f filter is a first order low pass filter. It is designed separately for each application as the inductor specifications are determined by the end user. The trans-conductance g_m and filter resistance R_f are variable. It is possible to change the frequency f_c by changing the value of R_f and to change the filter

gain by changing the value of g_m. The g_m-C_f filter gives accurate current measurement after tuning and calibration.

By applying voltage V_L to a g_m-C_f filter, whose voltage frequency response matches the current response of the inductor, one can write.

$$V_{Cf}(s) = g_m R_f \left(\frac{R_L + Ls}{1 + R_f C_f s} \right) I_L(s) \qquad (4.20)$$

If R_f is adjusted to match the both time constants (equation (4.10)), current I_L is given by (4.21).

$$I_L = \left(\frac{V_{Cf}}{(g_m R_f) R_L} \right) \qquad (4.21)$$

Here, $g_m R_f R_L$ is current sensing gain, which can be adjusted to any value by changing R_f and/or g_m. Tuning and calibration are performed during the start-up to adjust the filter gain-bandwidth product and filter dc gain for accurate current measurement, as shown in Figure 4.15.
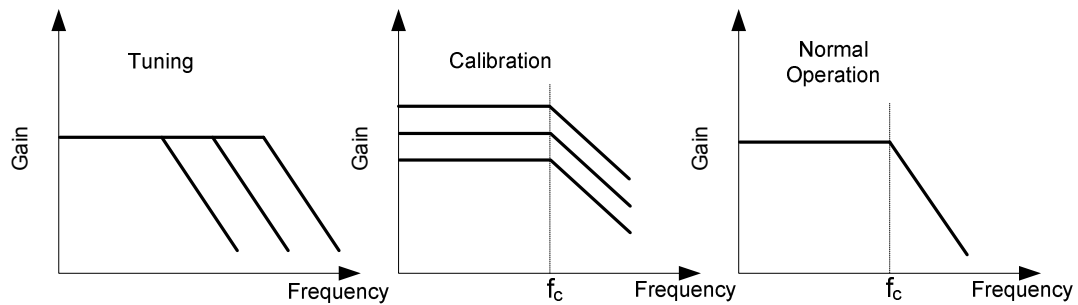
Figure 4.15. Tuning, calibration, and normal operation for filter-based current sensing technique

As tuning and calibration are performed during the start-up, switches S_1 and S_2 are kept disabled, so no power is lost during normal operation. This technique measures the inductor current during normal operation. Switches S_1 and S_2 are kept off and switches S_3 and S_4 are turned on during start-up for tuning purpose, as shown in Figure 4.14. A small ac test current ($I_O/20$), triangular in shape, is injected into the circuit, as shown in Figure 4.16.
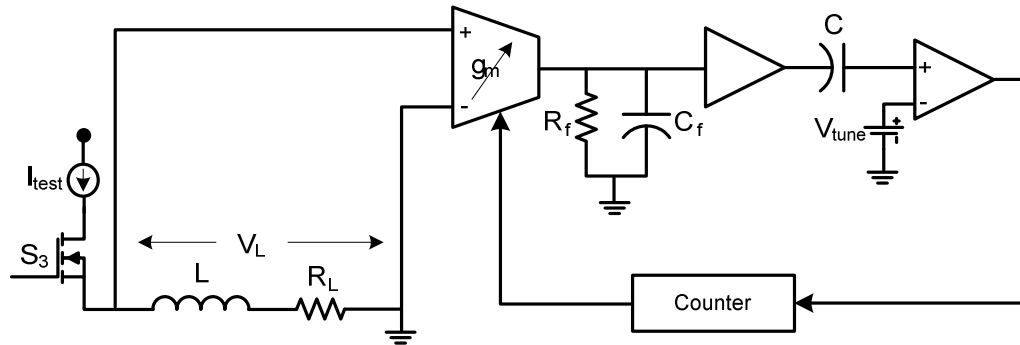
Figure 4.16. Tuning operation for filter-based current sensing technique

The test current's frequency is high enough that the voltage across inductor is dominated by inductance L and not by resistance R_L because inductor impedance is higher than resistance R_L at higher frequencies. The resulting ac voltage signal across inductor L is a square wave. The g_m-C_f filter converts this square wave voltage V_L into the triangular wave voltage V_L because capacitor impedance is smaller than resistance R_f at higher frequency. Resistor R_f is kept at its minimum value to reduce the dc offset during the tuning process. The filter output is then buffered and the dc component is removed. The peak of the ac portion of voltage V_{Cf} matches with the tune voltage V_{tune}

by adjusting g_m. Once both voltages are matched, the comparator stores their values and sends a stop signal to the counter.

The calibration phase immediately follows the tuning cycle. A small dc test current is supplied to the inductor for calibration, as shown in Figure 4.17. The value of filter resistance R_f is adjusted in the calibration process to match V_{Cf} with the calibration voltage V_{cali}.
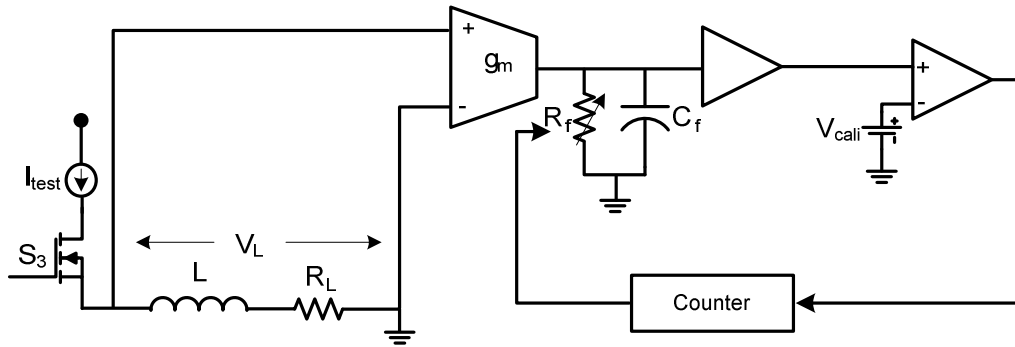
Figure 4.17. Calibration operation for filter-based current sensing technique

During tuning g_m-C_f filter's cutoff frequency is matched with the inductor's cutoff frequency, so (4.10) is satisfied. During the calibration process, the current sensing gain $g_mR_fR_L$ is adjusted to any value. If the value of the gain $g_mR_fR_L$ is set to 1 ohm, then the value of V_{Cf} can directly provide information about inductor current, as shown in (4.22).

$$I_L = V_{Cf} \tag{4.22}$$

Once tuning and calibration parameters are properly set and stored, the converter is allowed to operate normally.

4.3. COMPARISON BETWEEN CURRENT SENSING TECHNIQUES WITH SELF-TUNING AND/OR AUTO-CALIBRATION

Table 4.1 summarizes the advantages and disadvantages of the presented current sensing techniques with self-tuning and/or auto-calibration.

Table 4.1. Comparative overview of current sensing techniques with self-tuning and/or auto-calibration

Techniques	Advantages	Disadvantages
Using MOSFET R_{DS}-based current sensing with self-calibration	Lossless, accurate, combination of many lossless technique is also possible	Addition of an extra circuit, limited applications
Using filter-based current sensing	Lossless, continuous current measurement, low cost, low switching noise, high power efficiency	Low accuracy due to unknown L and R_L, filter design, temperature dependence, tolerance of components, time constant mismatching, only for off-chip applications, change in inductance due to dc current bias
Using filter-based current sensing with self-tuning	Lossless, accurate, matched time constants, continuous current measurement	Complicated circuit, filter design
Using combined-sense technique	Lossless, accurate, continuous current measurement, low cost, improved SNR	Complicated circuit, filter design, unmatched R_{DS} of main MOSFET switches, time constant mismatching
Using filter-based current sensing with self-tuning and self-calibration	Lossless, accurate, low switching noise, matched time constants, continuous current measurement, fully integrated	Complicated circuit, separate filter design for each application, accuracy of this technique depends on the tuning and calibration accuracy

5. AVERAGE CURRENT SENSING TECHNIQUES

It is hard to measure the instantaneous value of the current. In some applications, e.g. average current-mode control, there is no need to find the instantaneous value of current, only average value of current is enough. Different average current sensing techniques to calculate average inductor current are reviewed in this Section [39].

5.1. FILTER-BASED AVERAGE CURRENT SENSING

The simple, inexpensive, and efficient method of current sensing which measures the average value of the inductor current in a buck converter is depicted in Figure 5.1 [93, 151, 152,]. A simple R_fC_f filter is connected across low side switch S_2 of the buck converter for average current measurement.
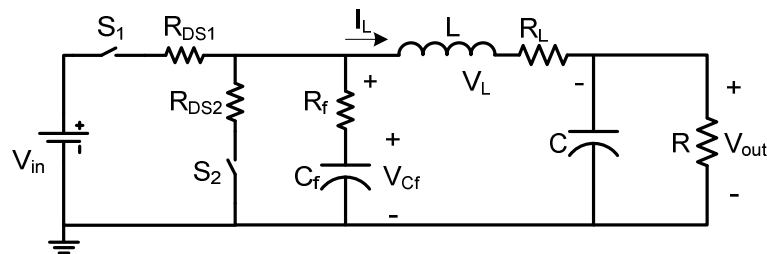
Figure 5.1. Filter-based average current sensing

Voltage V_L contains ac and dc parts. This technique measures the average voltage across the inductor, which is only a dc voltage across resistor R_L. Therefore, by measuring average inductor voltage, it is possible to measure average inductor current $<I_L>$.

The value of R_f is much greater than the values of switch resistances R_{DS1} and R_{DS2}. Another requirement of this technique is given by (5.1).

$$\tau_C \gg \tau_L \tag{5.1}$$

Where τ_C is a filter time constant and τ_L is an inductor time constant. When switch S_1 is on adnd S_2 is off, capacitor C_f is charged. Similarly, when switch S_2 is on and S_1 off, capacitor C_f is discharged. Under steady state, the voltage across capacitor C_f will be equal to the average voltage across switch S_2. Since the average current through resistor R_f is zero, the average capacitor voltage ($<V_{Cf}>$) is given by (5.2).

$$\langle V_{Cf} \rangle = V_{out} + \langle I_L \rangle R_L \tag{5.2}$$

From (5.2), current $<I_L>$ can be derived as (5.3).

$$\langle I_L \rangle = \frac{\langle V_{Cf} \rangle - V_{out}}{R_L} \tag{5.3}$$

From (5.3), it is inferred that the average inductor current is only affected by R_L. The value of R_f, C_f, L, and R_{DS} have no effect on the current-sensing result. This technique is used in interleaved parallel dc-dc converters to balance the average load currents in various channels.

This technique is useful for low frequency measurements only. Its main drawback is that, for accurate current sensing, the value of R_L must be known. This technique provides information about average current only; it does not give any information about ac currents or transients.

5.2. CURRENT TRANSFORMER-BASED AVERAGE CURRENT SENSING

Transformers are used to measure the "switched" current, not the "average" current delivered to the load. However, in this sub-section, different current sensing techniques using current transformers for average inductor current measurement are described [38, 153].

5.2.1. Average Current Measurement using Two Current Transformers. This technique uses two current transformers for average inductor current measurement. In a boost converter, two current transformers are used to sense the switch currents to measure average inductor current, as shown in Figure 5.2.
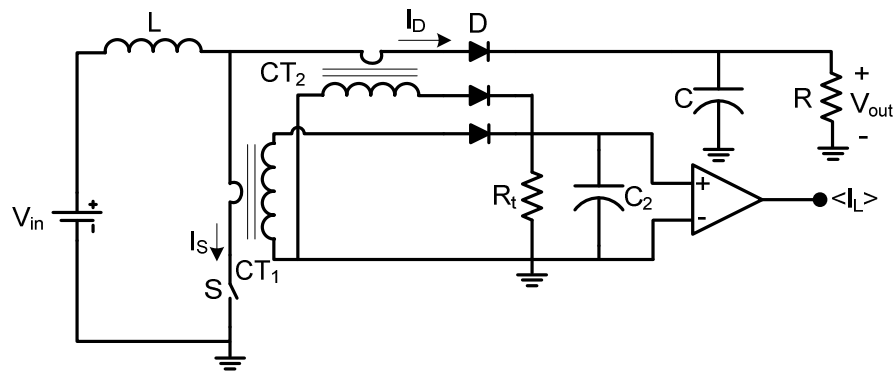
Figure 5.2. Average inductor current sensing using two current transformers

CT_1 measures switch current I_S and CT_2 measures diode current I_D. The outputs of the two CTs are then added to get the average value of the inductor current. Output is accurate both in waveform and in dc value. As the two transformers do not have same the number of turns, this method does not provide very accurate information about average current.

5.2.2. Average Current Measurement using One Current Transformer. This technique uses only one current transformer for average current measurement. Forward converter with one current transformer for average inductor current measurement is depicted in Figure 5.3.
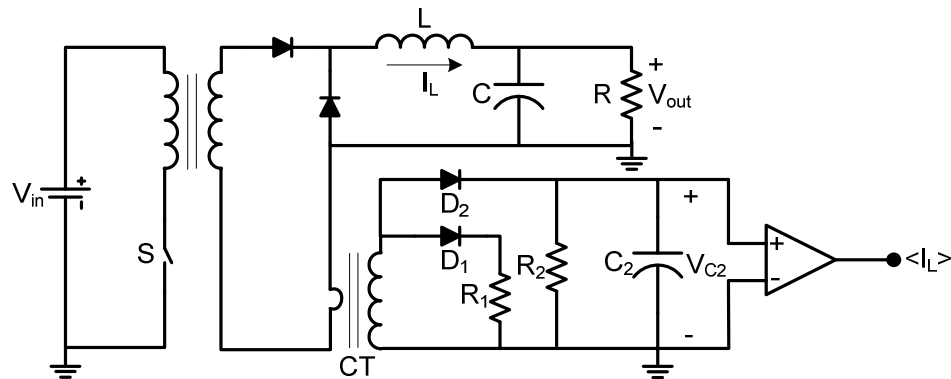
Figure 5.3. Average inductor current sensing using one current transformer

This technique replicates the inductor current waveform as capacitor voltage V_{C2} waveform. Voltage V_{C2} accurately follows the ac and dc excursion of inductor current. When switch S is on, the CT measures the inductor current. The output of CT is converted into the voltage using resistor R_1. This voltage is then used to charge capacitor C_2, which gives the rising portion of inductor current. When switch S is off, CT gets reset, and capacitor C_2 is discharged through resistor R_2, which gives the down-slope of the inductor current. The waveform for voltages V_{R1} and V_{C2} are given in Figure 5.4 to enable better understanding of this technique.
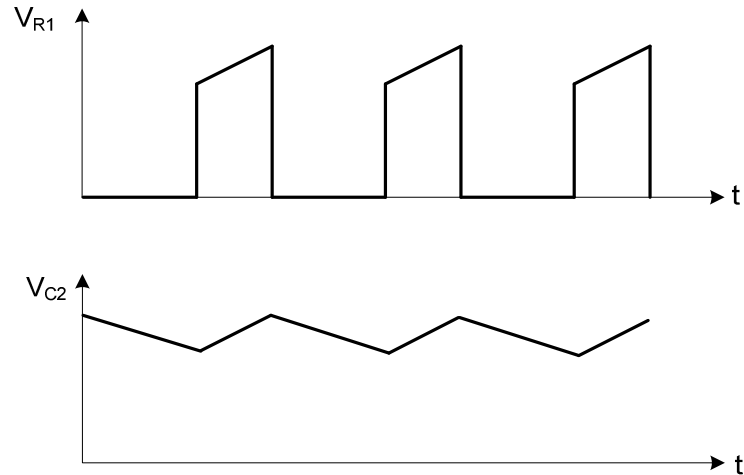
Figure 5.4. Voltage V_{R1} and V_{C2} for average current measurement

5.2.3. Average Current Sensing by Adding the Second Winding on the Existing Inductor. This technique mirrors the down-slope of the inductor current by using the second winding on the inductor, as depicted in Figure 5.5. The second winding generates the discharge current for capacitor C_2 through push-pull amplifier. By using inductor as CT, isolation is achieved with both charge and discharge signals.
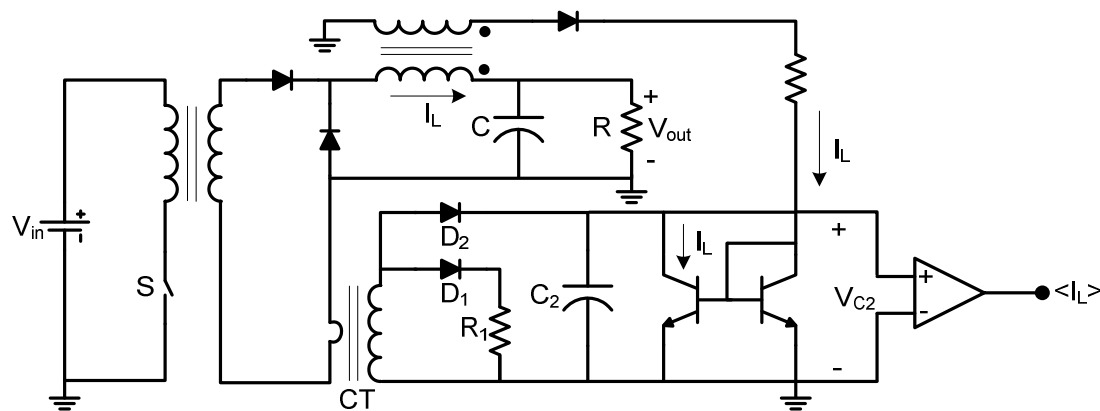
Figure 5.5. Average inductor current sensing by adding second winding on the existing inductor

In all of the above discussed techniques in this sub-section, the sensing circuits have their own grounds. Therefore, the sensing circuit can resides on either side of the isolation boundary.

5.3. COMPARISION BETWEEN AVERAGE CURRENT SENSING TECHNIQUES

Table 5.1 summarizes the advantages and disadvantages of the presented average current sensing techniques.

Table 5.1. Comparative overview of average current sensing techniques

Techniques	Advantages	Disadvantages
Using filter	Lossless, easily integrated on IC chip	Unknown R_L, information of average inductor current only, sensing dependence on R_f and C_f
Using two CTs	Simple, lossless	Requirement of two matched sensing transformers
Using one CT	Simple, lossless	Not very accurate, limited applications
Using inductor as a sense transformer	Simple, accurate, lossless	Additional winding expense, requirement of a high voltage approved isolation for off line converters

6. SUMMARY

Current measurement is a major contributor to the success in several applications. There are many applications for current sensing, including control, protection, monitoring, and power management. There are several issues related to current sensing, including ac or dc current measurement, complexity, linearity, sensitivity to switching noise, isolation requirements, accuracy, stability, robustness, bandwidth, transient response, cost, and acceptable power losses.

Current measurement is intrusive as there is a need to insert some type of sensor in the path of current flow for the current measurement. Most of the current measurement approaches can be categorized as resistive-based or electromagnetic-based techniques. In resistive-based current sensing techniques, the voltage drop across a sense resistor is measured to determine the current. These techniques have limited accuracy because the values of discrete elements of the circuit are unknown. Therefore, for accurate and continuous current measurement, different current sensing techniques with self-tuning and/or self-calibration are used. Electromagnetic-based current sensing techniques are used to measure current in high power applications where isolation is required. These techniques sense the magnetic field created by the current to be measured. Electromagnetic-based current sensing techniques are used to measure wide range of ac, dc, and complex currents with broad bandwidth.

Different current sensing strategies, such as resistive-based current sensing, electromagnetic-based current sensing, current sensing with self-tuning and/or auto-calibration, and average current sensing, are reviewed and evaluated in this thesis. Each

method has been introduced and its principle of operation is described. Different methods have been evaluated based on desirable characteristics. Several measurement techniques have been compared to each other, as well.

Applications of resistive-based and electromagnetic-based current sensing methods for low and high power circuits are listed in Table 6.1.

Table 6.1. Applications of resistive-based and electromagnetic-based current sensing techniques

Types of circuit	External R_{sense}	MOSFET-R_{DS}	Current sensing power MOSFET	Filter-based	CTs	Rogowski Coil	Hall-effect-based	Saturable inductor sensors	MR sensor	FOCS
Low power circuits										
• Battery charger					*		**			
• Voltage regulator modules			*	**						
• Electric vehicles							*		**	
• Power factor correction converters			*	**						
• Telecom applications					*					**
• Uninterruptible power supply				*			**			
• Control of power semiconductors						*		**		
High power circuits										
• Traction drive systems						**	*			
• Crusher and grinder motors						**	*			
• Converters for servo-motors					*		**			
• Current measurement for power analysis						**	*			
• Current measurement in busbar sets						**		*		
• High voltage distribution installations					*		**			
• Static converters for dc motor drives							**		*	

Resistive-based and electromagnetic-based current sensing techniques are suggested for particular application based on the criteria such as cost, linearity, sensor's space requirement, mass, operating range, isolation needs, bandwidth, response time, and type of current to be measured. In Table 6.1, '**' indicates the best technique that can be used for particular application and '*' indicates that one can use the particular technique for that application but it is not recommended. For example, in electric vehicle application, MR sensor is the best current measurement technique, however; one can also use Hall-effect-based sensors but they are not recommended due to their space requirement, weight, cost, and complexity.

BIBLIOGRAPHY

[1]   S. Wall, "Vector control: a practical approach to electric vehicles," *IEEE Colloquium Vector Control and Direct Torque Control of Induction Motors*, 1995.

[2]   J. Han-Su, K. Jang-Mok, K. Cheul-U, and C. Cheol, "Diminution of current measurement error for vector controlled AC motor drives," in *IEEE International Conference on Electrical Machines and Drives*, 15-18 May 2005, pp. 551-557.

[3]   S. Seung-Ho, C. Jong-Woo, and S. Seung-Ki, "Current measurement of digital field oriented control," in 31st *Industry Application Conference Annual Meeting*, 6-10 October 1996, vol. 1, pp. 334-338.

[4]   S. Chang and S. Yeh, "Current sensorless field-oriented control of induction motors," *IEE Electric Power Applications Proceedings*, vol. 143, pp. 492-500, November 1996.

[5]   M. Schroedl and R. Wieser, "EMF-based rotor flux detection in induction motors using virtual short circuits," *IEEE Transactions on Industry Applications*, vol. 34, pp. 142-147, January-February 1998.

[6]   H. Khalil and E. Strangas, "Robust speed control of induction motors using position and current measurements," *IEEE Transactions on Automatic Control*, vol. 41, pp. 1216-1220, August 1996.

[7]   S. Nonaka and Y. Neba, "Current regulated PWM-CSI induction motor drive system without a speed sensor," in *IEEE Conference Records of the Industry Applications Society Annual Meeting*, 4-9 October, vol. 1, pp. 347-354.

[8]   M. Rahman, M. Haque, T. Lixin, and Z. Limin, "Problems associated with the direct torque control of an interior permanent-magnet synchronous motor drive and their remedies," *IEEE Transactions on Industrial Electronics*, vol. 51, pp. 799-809, August 2004.

[9]   F. Colamartino, C. Marchand, and A. Razek, "Torque ripple minimization in permanent magnet synchronous servo drive," *IEEE Transactions Energy Conversion*, vol. 14, pp. 616-621, 1999.

[10]   E. Persson, "A new approach to motor drive current measurement," in *4th IEEE International Conference on Power Electronics and Drive Systems*, 22-25 October 2001, vol. 1, pp. 231-234.

[11]   S. Seung-Ho, C. Jong-Woo, and S. Seung-Ki, "Current measurements in digitally controlled AC drive," *IEEE Industry Applications Magazine*, vol. 6, pp. 51-62, July-August 2000.

[12]   D. Brod and D. Novotny, "Current control of VSI-PWM inverters," *IEE Transactions on Industry Applications*, vol. IA-21, pp. 562-570, May 1985.

[13]   J. Zamora and A. Garcia-Cerrada, "Online estimation of the stator parameters in an induction motor using only voltage and current measurements," *IEEE Transactions on Industry Applications*, vol. 36, pp. 805-816, May-June 2000.

[14]   M. Feemster, P. Aquino, D. Dawson, and D. Haste, "Sensorless rotor velocity tracking control for induction motors," in *IEEE American Control Conference Proceedings*, 2-4 June 1999, vol.3, pp. 2158-2162.

[15]   M. Tursini, R. Petrella, and F. Parasiliti, "Initial rotor position estimation method for PM motors," *IEEE Transactions on Industry Applications*, vol. 39, pp. 1630-1640, November-December 2003.

[16]   L. Sang Bin, K. Younsi, and G. Kliman, "An online technique for monitoring the insulation condition of AC machine stator windings," *IEEE Transactions on Energy Conversion*, vol. 20, pp. 737-745, December 2005.

[17]   Systems Control and Protection: Ensure the safety of door openers with current measurement - LEM.

[18]   B. Johansson, "Analysis of DC-DC converters with current-mode control and resistive load when using load current measurements for control," in *33rd Annual Power Electronics Specialist Conference*, 23-27 June 2002, vol. 1, pp. 165-172.

[19]   L. Dixon, "Average Current Mode Control of Switching Power Supplies," Texas Instruments. (Last visited: 7th November 2007)

[20]   M. Hartman, "Inside current-mode control," National Semiconductor. (Last visited: 7th November 2007)

[21]   C. Jiann-Jong, S. Juing-Huei, Y. Hung, C. Chung-Chieh, Y. Lee, and T. Chen, "Integrated current sensing circuit suitable for step-down dc-dc converters," in *35th IEEE Annual Power Electronics Specialist Conference*, 20-25 June 2004, vol. 2, pp. 1140-1140.

[22]   J. Chen, Y. Hwang, S. Juing-Huei, and S. Wei-Chung "New current sensing circuit for hysteresis-current-controlled buck converters," in *IEEE International Conference on Power Electronics and Drives Systems*, 16-18 January 2006, vol. 1, pp. 452-455.

[23] A. Peterchev and S. Sanders, "Load-line regulation with estimated load-current feedforward: application to microprocessor voltage regulators," *IEEE Transactions on Power Electronics,* vol. 21, pp. 1704-1717, November 2006.

[24] A. Prodic and D. Maksimovic, "Digital PWM controller and current estimator for a low-power switching converter," *7th Workshop on Computers in Power Electronics*, pp. 123-128, 16-18 July 2000.

[25] L. Peng and B. Lehman, "A design method for paralleling current mode controlled DC-DC converters," *IEEE Transactions on Power Electronics*, vol. 19, pp. 748-756, May 2004.

[26] Z. Mingjuan, D. Perreault, V. Caliskan, T. Neugebauer, S. Guttowski, and J. Kassal, "Design and evaluation of an active ripple filter with Rogowski-coil current sensing," in *30th Annual IEEE Power Electronics Specialists Conference*, vol. 2, 27th June – 1st July 1999, pp. 874-880.

[27] T. Bohn, R. Lorenz, and E. Olson, "Measurement of in-situ currents in a hybrid electric vehicle integrated power module using giant magnetoresistive sensors," *Power Electronics in Transportation*, pp. 55-59, 2004.

[28] S. Chakrabarti, T. Jahns, and R. Lorenz, "Current regulation for surface permanent-magnet synchronous motor drives using integrated current sensors in low-side switches," *IEEE Transactions on Industry Applications*, vol. 42, pp. 1080-1091, July-August 2006.

[29] Process and Quality Control Productivity Gain: Quality improvement and time savings thanks to current measurement - LEM. (Last visited: 7th November 2007)

[30] System Control and Protection: Generation yield improvement, control and protection in modern windmills - LEM. (Last visited: 7th November 2007)

[31] Z. Bin, A. Huang, Z. Xigen, L. Yunfeng, and S. Atcitty, "The built-in current sensor and over-current protection of the emitter turn-off (ETO) thyristor," in *IEEE Conference Record of the Industry Applications*, October 2003, vol. 2, pp. 1264-1269.

[32] R. Jayabalan and B. Fahimi, "Monitoring and fault diagnosis of cascaded multiconverter systems in hybrid electric vehicles," in *IEEE Vehicle Power and Propulsion Conference*, 7-9 September 2005.

[33] A. Peterchev, X. Jinwen, and S. Sanders, "Architecture and IC implementation of a digital VRM controller," *IEEE Transactions on Power Electronics*, vol. 18, pp. 356-364, January 2003.

[34]   O. Barbarisi, R. Canaletti, L. Glielmo, M. Gosso, and F. Vasca, "State of charge estimator for NiMH batteries," in *IEEE Conference on Decision and Control*, December 2002, vol.2, pp. 1739-1744.

[35]   B. Tsenter, "Battery management for hybrid electric vehicle and telecommunication applications," in *17th Annual Battery Conference on Applications and Advances*, 15- 18 January 2002, pp. 233-237.

[36]   Custom Power Solutions: State of charge (SOC) determination - Mpower. (Last visited: 7th November 2007)

[37]   Isolated current and voltage transducers: Characteristics, Applications, Calculations - LEM. (Last visited: 7th November 2007)

[38]   B. Mammano, "Current sensing solutions for power supply designers," Unitrode Design Note, Texas Instruments, 1997. (Last visited: 7th November 2007)

[39]   A. Patel and M. Ferdowsi, "Advanced Current Sensing Techniques for Power Electronic Converters," *IEEE Vehicular Power and Propulsion Conference,* Arlington, Texas, September 2007.

[40]   R. Lenk, "Application bulletin AB-20 optimum current sensing techniques in CPU converters," Fairchild Semiconductor Application Notes, 1999. (Last visited: 7th November 2007)

[41]   J. Sun, J. Zhou, M. Xu, and F. Lee, "A novel input-side current sensing method to achieve AVP for future VRs," *IEEE Transactions on Power Electronics*, vol. 21, pp. 1235-1242, September 2006.

[42]   H. Forghani-zadeh and G. Rincon-Mora, "Current-sensing techniques for DC-DC converters," *45th Midwest Symposium on Circuits and Systems*, vol. 2, August 2002, pp. II-577- II-580.

[43]   App Note 746: High-Side Current-Sense Measurement: Circuits and Principles - MAX4080. (Last visited: 7th November 2007)

[44]   Zetex AN39: Current Measurement Applications Handbook. (Last visited: 7th November 2007)

[45]   P. Givelin, M. Bafleur, T. Laopoulos, and S. Siskos, "On-chip over current and open load detection for a power MOS high-side switch: a CMOS current mode approach," in *5th European Conference on Power Electronics and Applications,* 13-16 September 1993, vol. 2, pp. 197-200.

[46] G. Rincon-Mora and H. Forghani-zadeh, "Accurate and lossless current-sensing techniques: A practical myth?" *Power Management Design Line (PMDL),* March 17, 2005.

[47] W. Ki, "Current sensing technique using MOS transistor scaling with matched current sources," US Patent-5757174.

[48] INT6566A Data Sheet: Three phase buck PWM controller with two integrated MOSFET drivers and one external driver signal, Intersil, 27 July 2005. (Last visited: 7th November 2007)

[49] H. Forghani-zadeh and G. Rincon-Mora, "A lossless, accurate, self-calibrating current-sensing technique for DC-DC converters," in *32nd Annual Conference of IEEE Industrial Electronics Society*, 6-10 November 2005.

[50] Y. Xiao, J. Cao, J. Chen, and K. Spring, "Current sensing trench power MOSFET for automotive applications," in *20th Annual IEEE Applied Power Electronics Conference and Exposition*, March 2005, vol. 2, pp. 766-770.

[51] A. Sedra, G. Roberts, and F. Gohh, "The current conveyor: history, progress and new results," *IEE Proceedings,* vol. 137, pp. 78-87, April 1990.

[52] D. Grant and R. Pearce, "Dynamic performance of current-sensing power MOSFETs," *Electronics Letters*, vol. 24, pp. 1129-1131, September 1988.

[53] P. Givelin, M. Bafleur, E. Tournier, T. Laopoulos, and S. Siskos, "Application of a CMOS current mode approach to on-chip current sensing in smart power circuits," *IEE Proceedings - Circuits, Devices and Systems*, vol. 142, pp. 357-363, December 1995.

[54] S. Yuvarajan and L. Wang, "Performance analysis and signal processing in a current sensing power MOSFET (SENSEFET)," in *IEEE Conference Record of the Industry Applications Society Annual Meeting*, 28th September – 4th October 1991, vol. 2, pp. 1445-1450.

[55] S. Clemente, H. Ishii, and S. Young, "International Rectifier AN-959: An introduction to the HEXSense current-sensing device." (Last visited: 7th November 2007)

[56] D. Grant and R. Williams, "Current sensing MOSFETs for protection and control," in *IEE Colloquium on Measurement Techniques for Power Electronics*, 22 October, pp. 8/1 – 8/5.

[57] M. Laxarus, K. Rabah, and P. Ripley, "Stabilised high power MOSFET modules," *IEE Proceedings, Communications, Speech, and Vision,* vol. 135, pp. 155-158, December 1988.

[58] P. Bimbhara, *Power Electronics*. Khanna Publisher, pp. 309-391, Chap. 8.

[59] "Introduction to BLDC motor drive power stage design - Part1," vol. 2, Hitachi America Ltd., February 2003. (Last visited: 7th November 2007)

[60] E. Persson and T.Takahashi, "Eliminate ripple current error from motor current measurement," Advance Development Group, International Rectifier Corp. (Last visited: 7th November 2007)

[61] V. Mangtani, "Current for sensing individual leg current in a motor controller using resistive shunts," US Patent – 5825641.

[62] P. O'Gorman and S. Repplinger, "Damping control in a three phase motor with single current sensor," US Patent – 20050248361.

[63] F. Blaabjerg and J. Pedersen, "Modulation and current sensing technique an integrated part for low-cost motor-drive," *Proceedings of the IEEE International Industrial Electronics,* vol. 1, pp. 476-481, 17-20 June.

[64] A. Clothier and B. Mecrow, "Inverter topologies and current sensing methods for short pitched and fully pitched winding SR motor," in *Applied Power Electronics Conference and Exposition,* March 1999, vol.1, pp. 416-423.

[65] T. Green and W. Williams, "Derivation of motor line-current waveforms from the DC-link current of an inverter," *IEE Proceedings – Electric Power Applications*, vol. 136, pp. 196-204, July 1989.

[66] H. Tan and S. Ho, "A novel single current sensor technique suitable for BLDCM drives," *Proceedings of the IEEE Power Electronics and Drive Systems,* vol.1, pp. 133-138, 27-29 July 1999.

[67] F. Parasiliti, R. Petrella, and M. Tursini, "Low cost phase current sensing in DSP based AC drives," *Proceedings of the IEEE International Symposium on Industrial Electronics,* vol.3, pp. 1284-1289, 12-16 July 1999.

[68] C. Zhang and F. Lin, "A single current sensor control technique for induction motors," in *International Conference on Power System Technology,* 13-17 October 2002, vol.4, pp. 2290-2293.

[69] J. Boys, "Novel current sensor for PWM AC drives," *IEE Proceedings B- Electric Power Applications,* vol. 135, pp. 27-32, January 1988.

[70] F. Blaabjerg and J. Pedersen, "A new low-cost, fully fault-protected PWM-VSI inverter with true phase-current information," *IEEE Transactions on Power Electronics,* vol. 12, pp. 187-197, January 1997.

[71]   P. Acarnley, "Current measurement in three-phase brushless DC drives," *IEE Proceedings B- Electric Power Applications,* vol. 140, pp. 71-79, January 1993.

[72]   F. Blaabjerg, J. Pedersen, U. Jaeger, and P. Thoegersen, "Single current sensor technique in the DC link of three-phase PWM-VS inverters: a review and a novel solution," *IEEE Transactions on Industry Applications*, vol. 33, pp. 1241-1253, September-October 1997.

[73]   T. Green and B. Williams, "Derivation of motor line-current waveforms from the DC-link current of an inverter," *IEE Proceedings B- Electric Power Applications,* vol. 136, pp. 196-204, July 1989.

[74]   S. Vukosavic and A.Stankovic, "Sensorless induction motor drive with a single DC-link current sensor and instantaneous active and reactive power feedback," *IEEE Transactions on Industrial Electronics,* vol. 48, pp. 195-204, February 2001.

[75]   H. Kim and T. Jahns, "Phase current reconstruction for AC motor drives using a DC-link single current sensor and measurement voltage vectors," *IEEE Transactions on Power Electronics,* vol. 21, pp. 1413-1419, September 2006.

[76]   App Note 1121: Practical layout for current sensing circuit of IRMCF300 series IC - International Rectifier. (Last visited: 7th November 2007)

[77]   M. Armstrong, D. Atkinson, C. Johnson, and T. Abeyasekera, "Auto-Calibrating DC Link Current Sensing Technique for Transformerless, Grid Connected, H-Bridge Inverter Systems," *IEEE Transactions on Power Electronics*, vol. 21, pp. 1385-1393, September 2006.

[78]   H. Wang, S. Pekarek, and B. Fahimi, "Elimination of position and current sensors in high performance adjustable speed ac drives," *IEEE International Conference on Electric Machines and Drives,* 15-18 May 2005, pp. 1902-1911.

[79]   J. Shao, "An Improved microcontroller-based sensorless brushless DC (BLDC) motor drive for automotive applications," in *40th IAS Annual Industry Applications Conference,* 2-6 October, vol.4, pp. 2512-2517.

[80]   AND8093/D: Current sensing power MOSFET - ON Semiconductor. (Last visited: 7th November 2007)

[81]   Ideas for Design: Small and medium power MOS transistors - Phillips Semiconductors. (Last visited: 7th November 2007)

[82]   S. Chakrabarti, T. Jahns, and R. Lorenz, "A current control technique for induction machine drives using integrated pilot current sensors in the low-side switches," in *IEEE Power Electronics Specialists Conference,* Aachen, Germany, June 2004.

[83]   S. Chakrabarti, T. Jahns, and R. Lorenz, "A current reconstruction algorithm for three-phase inverters using integrated current sensor as low side switches," *IEEE Industry Applications Society Annual Meeting*, Salt Lake City, UT, pp. 925-932, October 2003.

[84]   S. Chakrabarti, T. Jahns, and R. Lorenz, "Reduction of parameter sensitivity in an induction motor current regulator using integrated pilot current sensors in the low-side switches," *IEEE Industrial Application Society Annual Meeting*, Seattle, WA, pp. 647-654, October 2004.

[85]   T. Jahns and E. Wildi, "Integrated current sensor configurations for AC motor drives," U.S Patent 4777579.

[86]   T. Chow, D. Pattanayak, E. Wildi, J. Pimbley, B. Baliga, and M. Adler "Design of current sensors in IGBT's," in *Proceedings of Device Research Conference,* Boston, MA, June 1992.

[87]   M. Ehsani, I. Husain, and A. Kulkarni, "Elimination of discrete position sensor and current sensor in switched reluctance motor drives," *IEEE Transactions on Industry Applications,* vol. 28, pp. 128-135, January-February 1992.

[88]   S. Yuvarajan and L. Wang, "Power conversion and control using a current sensing power MOSFET," *34th Midwest Symposium on Circuits and Systems*, vol.1, pp. 166-169, 14-17 May 1991.

[89]   K. Bilings, *Switch Mode Power Supply Handbook.* McGraw-Hill Publishing Company, pp. 3.176-3.192, 1989, Chap. 14.

[90]   W. Hays, "Exploring Current Transformer Applications," BH Electronics, Marshall, Minnesota. (Last visited: 7th November 2007)

[91]   App Note 0305: Introduction to current transformers - Elkor Technologies Inc. (Last visited: 7th November 2007)

[92]   B. Theraja and A. Theraja, *A Textbook of Electrical Technology in SI Units.* S. Chand and Co., vol.2, pp. 1115-1242, 2006, Chap. 32 and 33.

[93]   H. Marecar and R. Oruganti, "Fast and accurate current sensing in a multiphase buck converter," in *IEEE International Conference on Power Electronics and Drives Systems,* 16-18 January 2006, vol.1, pp. 166-171.

[94] W. Leung-Pong, L. Yim-Shu, and D. Cheng, "Bi-directional pulse-current sensors for bi-directional PWM DC-DC converters," in *31st IEEE Annual Power Electronics. Specialists Conference*, 18-23 June 2000, vol. 2, pp. 1043-1046.

[95] M. Kwok-Wai and L. Yim-Shu, "Technique for sensing inductor and DC output currents of PWM DC-DC converter," *IEEE Transactions on Power Electronics,* vol. 9, pp. 346-354, May 1994.

[96] M. Kwok-Wai and L. Yim-Shu, "Novel technique for sensing inductor and DC output currents of PWM DC-DC converter," in *7th Annual Applied Power Electronics Conference Proceedings,* 23-27 February 1992, pp. 345-351.

[97] N. McNeill, N. Gupta, and W. Armstrong, "Active current transformer circuits for low distortion sensing in switched mode power converters," *IEEE Transactions on Power Electronics*, vol. 19, pp. 908-917, July 2004.

[98] J. Petter, J. McCarthy, P. Pollak, and C. Smith, "Survey of DC current measurement techniques for high current precision power supplies," in *IEEE Nuclear Science Symposium and Medical Imaging Conference*, 2-9 November 1991, vol. 2, pp. 961-967.

[99] E. Laboure, F. Costa, and F. Forest, "Current measurement in static converters and realization of a high frequency passive current probe (50 A-300 MHz)," in *5th European Conference on Power Electronics and Applications*, 13-16 September 1993, vol. 4, pp. 478-483.

[100] H. Strom, *Magnetic Amplifiers*. Wiley and Sons, 1955, pp. 79, 167, 407.

[101] A. Radun, "An alternative low-cost current-sensing scheme for high-current power electronic circuits," *IEEE Transactions on Industrial Electronics*, vol. 42, pp. 78-84, February1995.

[102] D. Ward and J. Exon, "Experience with using Rogowski coils for transient measurements," *IEE Colloquium on Pulsed Power Technology,* pp. 6/1-6/4, 20 February 1992.

[103] D. Ward and J. Exon, "Using Rogowski coils for transient current measurements," Engineering Science and Education Journal. (Last visited: 7th November 2007)

[104] G. Xiaohua, Y. Miaoyuan, X. Yan, Z. Mingjun, and L. Jingsheng, "Rogowski current transducers suit relay protection and measurement," in *IEEE International Conference on Power System Technology,* 13-17 October 2002, vol.4, pp. 2617-2621.

[105] A. Luciano and M. Savastano, "Wide band transformer based on a split-conductor current sensor and a Rogowski coil for high current measurement," in *IEEE Instrumentation and Measurement Technology Conference,* 24-26 April, pp. 454.

[106] X. Chucheng, Z. Lingyin, T. Asada, W. Odendaal, and J. van Wyk, "An overview of integratable current sensor technologies," in *38th Industry Applications Conference Meeting,* 12-16 October, vol.2, pp. 1251-1258.

[107] M. Imamura, M. Nakahara, T. Yamaguchi, and S. Tamura, "Analysis of magnetic fields due to three-phase bus bar currents for the design of an optical current transformer," *IEEE Transactions on Magnetics*, vol.4, pp. 2274-2279, July 1998.

[108] P. Wang, G. Zhang, X. Zhu, and C. Luo, "Planar Rogowski Coil current transducer used for three-phase plate-form busbars," in *IEEE Instrumentation and Measurement Technology Conference Proceedings,* 1-3 May, pp. 1-4.

[109] M. Imamura, M. Nakahara, and S. Tamura, "Output characteristics of field sensor used for optical current transformers applied to the flat-shape three-phase bus-bar," *IEEE Transactions on Magnetics*, vol.33, pp. 3403-3405, September 1997.

[110] E. Favre and W. Teppan, "Sate of the art in current sensing technologies," in *Proceedings Power Electronics Intelligent Motion Conference*, November 2003, pp. 549-554.

[111] R. Dickinson, and S. Milano, "Isolated open loop current sensing using Hall Effect technology in an optimized magnetic circuit," Allegro MicroSystems, Inc. (Last visited: 7th November 2007)

[112] J. Pankau, D. Leggate, D. Schlegel, R. Kerkman, and G. Skibiniski, "High-frequency modeling of current sensors," *IEEE Transactions on Industry Applications*, vol.35, pp. 1374-1382, November – December 1999.

[113] K. Corzine and D. Sudhoff, "A hybrid observer for high performance brushless DC motor drives," *IEEE Transactions on Energy Conversion,* vol. 11, pp. 318-323, June 1996.

[114] T. Matsuo, V. Blasko, J. Moreira, T. Lipo, "Field oriented control of induction machines employing rotor end ring current detection," *IEEE Transactions on Power Electronics*, vol. 9, pp. 638-645, November 1994.

[115] C. Chunshan, J. wang, G. Cao, and X. Zhao, "Design of a new current sensing device for joint torque force control of the precision assembly robot," *5th World Congress on Intelligent Control and Automation,* vol.5, pp. 4609-4613, June 2004.

[116] LEM Current Sensors 2007 [Online]. Available: *www.lem.com* (Last visited: 7th November 2007)

[117] Hall Effect Current Sensors 2007 [Online]. Available: *www.bbautomacao.com* (Last visited: 7th November 2007)

[118] Current Measurement 2007 [Online]. Available: *www.sypris.com* (Last visited: 7th November 2007)

[119] L. Ghislanzoni and J. Carrasco, "A DC current transformer for large bandwidth and high common-mode rejection," *IEEE Transactions on Industrial Electronics,* vol. 46, pp. 631-636, June 1999.

[120] D. Leggate, J. Pankau, R. Kerkman, D. Schlegel, and G. Skibiniski, "Reflected waves and their associated current," *IEEE Transactions on Industry Applications,* vol. 35, pp. 1383-1392, November – December 1999.

[121] Technical Information: Closed Loop Transducers with small footprint up to 100A nominal - LEM. (Last visited: 7th November 2007)

[122] R. Major, "Current measurement with magnetic sensors," *IEE Colloquium on Magnetic Materials for Sensors and Actuators,* pp. 5/1-5/3, 11 October 1994.

[123] Technical Information: Transducers with Eta technology up to 50 and 100A nominal - LEM. (Last visited: 7th November 2007)

[124] L. Dalessandro, N. Karrer, and J. Kolar, "High-performance planar isolated current sensor for power electronics applications," *IEEE Transactions on Power Electronics,* vol.22, pp. 1682-1692, September 2007.

[125] J. Carrasco, E. Sanchis-Kilders, D. Ramirez, and E. Dede, "Improved magnetic coupled current sensing techniques," *27th Annual IEEE Power Electronics Specialists Conference*, 23-27 June 1996, vol.1, pp. 829-834.

[126] Technical Information: CTs ITB 300-S, IT 400-S and IT 700-S high accuracy - high technology - simply the perfect choice - LEM. (Last visited: 7th November 2007)

[127] E. Olson and R. Lorenz, "Integrating giant magnetoresistive current and thermal sensors in power electronic modules," in *18th Annual IEEE Applied Power Electronics Conference and Exposition,* 9-13 February, vol. 2, pp. 773-777.

[128] D. Alfano and T. Dupuis, "Current sensor with reset circuit," US Patent – 2007/0139835. (Last visited: 7th November 2007)

[129] Z. Heinz Lienhard, O. Jan Petr, and Z. Benedikt Steinle, "Magnetoresistive current detector," US Patent 4464625.

[130] H. Mason, "Basic introduction to the use of magnetoresistive sensors," App Note 37, Zetex Semiconductors. (Last visited: 7th November 2007)

[131] G. Laimer and J. Kolar, "Design and experimental analysis of a DC to 1 MHz closed loop magnetoresistive current sensor," in *20th Annual IEEE Applied Power Electronics Conference and Exposition,* 6-10 March, vol.2, pp. 1288-1292.

[132] P. Mihailovic, S. Petricevic, Z. Stojkovic, and J. Radunovic, "Development of a portable fiber-optic current sensor for power systems monitoring," *IEEE Transactions on Instrumentation and Measurement,* vol. 53, issue 1, pp. 24-30, February 2004.

[133] J. Blake, "Fiber optic current sensor calibration," in *IEEE/PES Transmission and Distribution Conference and Exposition*, vol. 1, 28 October-2 November 2001, pp. 127-130.

[134] J. Blake and A. Rose, "Fiber-optic current transducer optimized for power metering applications," in *IEEE PES Transmission and Distribution Conference and Exposition,* vol. 1, 7-12 September 2003, pp. 405-408.

[135] P. Niewczas, W. Madden, W. Michie, A. Cruden, J. McDonald, "Magnetic crosstalk compensation for an optical current transducer," *IEEE Transactions on Instrumentation and Measurement,* vol. 50, issue 5, pp. 1071-1075, October 2001.

[136] E. Vaerewyck and E. Anderson, "Electric motor and transformer load sensing technique," US Patent – 4428017.

[137] B. Bryant and M. Kazimierczuk, "Effect of a current-sensing resistor on required MOSFET size," *IEEE Transactions on Circuit and Systems I: Fundamental Theory and Applications,* vol. 50, pp. 708-711, May 2003.

[138] Z. Yang, R. Zane, A. Prodic, R. Erickson, and D. Maksimovic, "Online calibration of MOSFET on-state resistance for precise current sensing," *IEEE Power Electronics Letter*s, vol. 2, pp. 100-103, September 2004.

[139] Z. Yang, R. Zane, A. Prodic, R. Erickson, and D. Maksimovic, "On-line calibration of lossless current sensing," in *19th Annual IEEE Applied Power Electronics Conference and Exposition*, vol. 2, 2004, pp. 1345-1350.

[140] E. Dallago, M. Passoni, and G. Sassone, "Lossless current sensing in low-voltage high-current DC/DC modular supplies," *IEEE Transactions on Industrial Electronics*, vol. 47, pp. 1249-1252, December 2006.

[141] D. Yan, X. Ming, and F. Lee, "DCR current sensing method for achieving adaptive voltage positioning (AVP) in voltage regulators with coupled inductors," in *37th IEEE Power Electronics Specialists Conference,* 18-22 June 2006, pp. 1-7.

[142] S. MacMinn, W. Rzesos, P. Szczesny, and T. Jahns, "Application of sensor integration techniques to switched reluctance motor drives," *IEEE Transactions on Industry Applications,* pp. 1339 – 1344, vol.28, November-December 1992.

[143] H. Lei and L. Shiguo, "Design considerations of time constant mismatch problem for inductor DCR current sensing method," in *21st Annual IEEE Applied Power Electronics Conference and Exposition,* 19-23 March 2006.

[144] N. Ismail, "Two phase buck converter with integrated high current 5V to 12V drivers," Intersil Application Note 1197, ISL6310EVAL1Z. (Last visited: 7th November 2007)

[145] LINFINITY Application Note AN-7: A simple-current sense technique eliminating a sense resistor. (Last visited: 7th November 2007)

[146] G. Garcea, S. Saggini, D. Zambotti, and M. Ghioni, "Digital auto-tuning system for inductor current sensing in VRM applications," in *21st Annual IEEE Applied Power Electronics Conference and Exposition*, 19-23 March 2006.

[147] C. Chang, "Combined lossless current sensing for current mode control," in *19th Annual IEEE Applied Power Electronics Conference and Exposition*, 2004, vol. 1, pp. 404-410.

[148] P. Lethellier, "Method and apparatus for sensing output inductor current in a dc-to-dc power converter," US patent 6441597B1.

[149] H. Forghani-zadeh and G. Rincon-Mora, "An Accurate, Continuous, and Lossless Self-Learning CMOS Current-Sensing Scheme for Inductor-Based DC-DC Converters," *IEEE Journal of Solid-State Circuits*, March 2007, vol. 42, pp. 665-679.

[150] An integrated, lossless, and accurate current- sensing system for high-performance dc-dc converters, *Microsoft PowerPoint - gtac_s04.ppt* (Last visited: 7th November 2007)

[151] Z. Xunwei, X. Peng, and F. Lee, "A novel current-sharing control technique for low-voltage high-current voltage regulator module applications," *IEEE Transactions on Power Electronics,* pp. 1153-1162, vol. 15, November 2000.

[152]   Z. Xunwei, P. Xu, and F. Lee, "A high power density, high efficiency and fast transient voltage regulator module with a novel current sensing and current sharing technique," in *14th Annual Applied Power Electronics Conference and Exposition*, pp. 289-294, vol. 1, 14-18 March 1999.

[153]   J. O'Connor, "The UC3848 average current mode controller squeezes maximum performance from single switch converters," Unitrode Application Note-135. (Last visited: 7th November 2007)

VITA

      Ashaben Mehul Patel was born on May 3, 1981, in Gujarat, India. She received her primary and secondary education in India. She earned her Bachelor of Engineering degree in Electrical Engineering from Sardar Vallabhbhai National Institute of Technology, Surat, India in June of 2002. She worked for two years as a Lecturer in the Diploma Engineering College in India. Patel became a Graduate student in Electrical Engineering at the University of Missouri-Rolla in the spring of 2006. She held a Graduate Research Assistantship under Dr. Mehdi Ferdowsi with the Department of Electrical Engineering at the University of Missouri-Rolla. She completed an internship at Dow Chemical Company of Houston, Texas, in the summer of 2007. Patel received her Master of Science degree in Electrical Engineering from the University of Missouri-Rolla in December of 2007.